1-1-2003

Theoretical study of segregation kinetics of indium in indium gallium nitride and magnesium in magnesium-gallium nitride grown by molecular beam epitaxy

Irena Vidhya Mabel Stanley
University of Nevada, Las Vegas

THEORETICAL STUDY OF SEGREGATION KINETICS OF *In* IN *InGaN* AND *Mg* IN *Mg-GaN* GROWN BY MOLECULAR BEAM EPITAXY

by

Irena Vidhya Mabel Stanley

Bachelor of Science
University of Madras, India
2001

A thesis submitted in partial fulfillment
of the requirements for the

Master of Science Degree in Engineering
Department of Electrical and Computer Engineering
Howard R. Hughes College of Engineering

Graduate College
University of Nevada, Las Vegas
May 2003

UMI Number: 1414551

UMI®

UMI Microform 1414551

ProQuest Information and Learning Company
300 North Zeeb Road
P.O. Box 1346
Ann Arbor, MI 48106-1346

UNLV
UNIVERSITY OF NEVADA LAS VEGAS

Thesis Approval
The Graduate College
University of Nevada, Las Vegas

April 11, 2003

The Thesis prepared by

Irena Vidhya Mabel Stanley

Entitled

"Theoretical Study of Segregation Kinetics of In in InGan and Mg in Mg-GaN Grown by Molecular Beam Epitaxy"

is approved in partial fulfillment of the requirements for the degree of

Master of Science

Examination Committee Chair

Dean of the Graduate College

Examination Committee Member

Examination Committee Member

Ajay Kumar Datta

Graduate College Faculty Representative

1017-53

ABSTRACT

Theoretical Study of Segregation Kinetics of *In* in *InGaN* and *Mg* in *Mg-GaN* Grown by Molecular Beam Epitaxy

by

Irena Vidhya Mabel Stanley

Dr. Rama Venkat, Examination Committee Chair
Professor of Electrical and Computer Engineering
University of Nevada, Las Vegas

A rate equation model including all physically relevant surface processes is developed for the study of *In* segregation in *InGaN* and *Mg* segregation in *Mg-GaN* MBE growth. In *InGaN* growth, the simulations were carried for a variety of growth conditions spanning the growth parameter space: substrate temperature in the range of 500-700 ^oC; *Ga* flux in the range of 1.17-8.98 *nm/min*; *In* flux in the range of 0.39-28.74 *nm/min* and *N* flux in the range of 4.7-12 *nm/min*. Results of *In* incorporation obtained from simulations are within 1% agreement with the experiments reported in the literature. *In* segregation is found to be negligible below 580 ^oC. Above 640 ^oC, the segregation dominates the kinetics. This temperature dependence is found to be independent of the fluxes. In *Mg-GaN* growth, simulations were carried for various growth temperatures in the range of 600-750 ^oC with constant flux rates of *Mg*, *Ga* and *N*. For the given flux rates, it is found that *Mg* segregates to the surface with the increase in temperature. Above 750 ^oC a dopant depleted zone is formed below the surface layer. Results obtained from simulations are in good qualitative agreement with the experimental data.

TABLE OF CONTENTS

LIST OF FIGURES

ACKNOWLEDGEMENTS

I am obliged to my advisor, Dr. Rama Venkat, for his invaluable guidance and support throughout my academic years. I acknowledge his warmth and patience in persuading me to bring forward this work. I am indebted to him forever.

I thank Dr. Shahram Latifi, Dr. Sahjendra Singh and Dr. Ajoy K. Datta for having accepted to serve in my examination committee. I acknowledge the financial support from AFOSR through DEPSCoR 99 under contract # F49620-99-1-0188.

I owe my parents for their love, support and encouragement and also for their great efforts in bestowing me the best possible education. I express my sincere thanks and love to my uncle, for without him I would not have attained this level of education. I appreciate my sister for her love and support. Thanks are due to all my friends in UNLV, especially Supriya Kamaraju and Preethi Linga, for their moral support.

CHAPTER 1

INTRODUCTION

Molecular Beam Epitaxy is the leading technique in growing high purity and atomistically controlled hetero-epitaxial layers [1]. The process involves the crystallization of compounds on the substrate by the process of condensation and reaction of vapor in ultra high vacuum. The inner surfaces of MBE growth chamber are very clean as the chamber is evacuated to high vacuum level up to 10^{-10} torr. The high purity hetero-structures for device applications of controlled composition and thickness can be grown by MBE due to low growth rates of the order of $1\mu m/hr$. Since the molecules in the beam don't collide with each other before they reach the substrate surface, multi-layered structures with abrupt interfaces and compositional changes can be grown.

The in-situ monitoring techniques such as Auger Spectroscopy and Reflection High Energy Electron Diffraction (RHEED) available in MBE systems make it a highly efficient process tool. The growing surface is monitored as it grows and the composition, thickness, crystallinity and roughness can be dynamically controlled. The precise control of beam fluxes, growth conditions and the in-situ monitoring makes MBE a versatile growth technique, which is more reliable than all others. MBE technique has been used successfully in growing a variety of electronic and opto-electronic devices involving a variety of IV, III-V and II-VI compounds and their alloys. The materials used extensively are *GaAlAs*, *InGaP*, *HgCdTe* and *GaAlN*.

Highly efficient light emitting diodes and lasers are fabricated using III-nitride semiconductors [2]. The reason for their prominence in blue lasers and LEDs is their large band gap. In addition, using various III-nitride compounds with bandgap spanning the whole of visible spectrum, opto-electronic devices in all three primary colors can be fabricated. Group III-nitrides are the choice for the opto-electronic devices due to higher device stability for high temperature and high break down fields than the II-VI *ZnSe* based devices. The recent successful realization of semiconductor light emitting diodes and lasers commercially has paved way for increased interest in thin films wide band gap III-N.

In spite of the increased interest and successful device fabrication [3-20], the precise understanding of the atomistic details of the growth process is lacking. Such details are necessary for reproducing the hetero-structures with abrupt interfaces and varying compositions. Attempts at theoretical modeling of growth included Stochastic models [21, 22], Monte Carlo simulations [23, 24], Quasi thermodynamic models [25, 26, 27] and Rate equation models [28, 29, 30]. Each approach has some advantages and limitations compared to the other. Details of these are presented in Section 2, Literature Survey.

Chen *et. al.* [31] and Averbeck *et. al.* [32] investigated the growth kinetics of *InGaN* and its relation to growth conditions such as temperature and fluxes. In both their work, it was observed that *In* segregates to surface at high temperatures independent of the fluxes and flux ratios due to the weaker bond strength of *InN* compared to *GaN.*

Guha *et. al.* [33], Myoung *et. al.* [34] and Cheng *et. al.* [35, 36] studied the mechanism of Magnesium incorporation and segregation in *GaN* grown by MBE. The

effect of flux ratio and substrate temperature was investigated and it was observed that *Mg* segregates to the surface through inter layer migration due to the rapid diffusion of *Mg* and the dependence of its diffusion rate on substrate temperature and incident flux rate.

In spite the experimental work presented in Ref. [31, 32, 33, 34, 35], a clear understanding of the segregation phenomena is lacking. In this thesis work, the rate equation model developed and used by Fu *et. al.* [37] is adopted and modified to study the segregation phenomenon and the underlying physics and chemistry. Segregation of *In* in *InGaN* and *Mg* in *GaN* are studied in their relation to the growth conditions. The models simulated in this work can be developed as software and can be used in the industry, through which the overall cost of crystal production can be minimized.

1.1 Organization Of The Thesis

In Chapter 2, the literature review on MBE, group III-nitrides, *InGaN*, doping issues, models and devices are presented. In chapter 3, a detailed rate equation model including all the appropriate surface processes, is developed for the theoretical study of growth of *InGaN* and *Mg* doped *GaN* by molecular beam epitaxy. Also the computational details and model parameters are presented in chapter 3. The results and discussions are presented in chapter 4. Conclusions are in chapter 5.

CHAPTER 2

LITERATURE REVIEW

2.1 Molecular Beam Epitaxy

The Molecular Beam Epitaxy (MBE) systems can be physically divided into three zones [1]. Each of these zones plays an important role in the growth of an epilayer and any alterations in these zones will seriously impact the growth.

In the first zone the generation of molecular beam is accomplished. The molecular beams are generated from Knudsen effusion cells (K-cells) under ultra high vacuum of the order of 10^{-9} torr. Flux from the K-cell is controlled by the shutters situated at the mouth of the cell, which is electronically controlled from outside. The desired composition in the epitaxial film can be obtained by appropriately opening and closing the shutters of particular K-cells and by choosing the particular substrate temperature. The spatial uniformity of the molecular fluxes from the K-cells controls the spatial variation of the thickness on the wafer. The effusion cells are made in various sizes and shapes according to the needs of the technology.

The second zone is the vacuum area through which the molecular beam travels and reaches the substrate. The mean free paths of the molecules are long such that they do not collide during their flight from the K-cell to the substrate. Thus, the molecules do not exhibit viscous flow. At the periphery of this zone, the in-situ growth monitoring tools

such as Auger Spectroscopy and Reflection High Energy Electron Diffraction (RHEED) are also situated.

The third zone is the area where the crystallization occurs on the substrate due to interaction of molecular beams at the substrate temperature. Various surface processes take place in this area that result in the growth of the epilayer. The surface processes are: adsorption, surface migration and dissociation of the adsorbed molecules, incorporation and thermal desorption. The adsoprtion is of two types. One is physisorption in which the adsorbate is bonded to the substrate through weak bonds (Vander waals force) and no electron transfer between the atoms is involved. The other is chemisorption in which the adsorbate and substrate chemically react and transfer of electrons between the atoms is involved. Van der Waal bonding is of the order of 0.1-0.2 eV whereas the chemical bonding is typically 1-2 eV.

The in-situ monitoring is done by RHEED (Reflection High Energy Electron Diffraction), REMS (Reflection Mass Spectrometry), MBMS (Modulated Beam Spectrometry), and RDS (Reflectance Difference Spectroscopy). RHEED is used to monitor the crystal structure and the microstructure of the growing surfaces. REMS and MBMS are used to monitor the surface chemistry and composition on the growing surface. RDS is used to monitor the composition through the optical properties of the growing surfaces.

Ellipsometry and laser interferometry are other optional techniques that are used. Since these in-situ techniques do not interfere with the flow of molecular flux or beams, they are non destructive and provide the direct measurement of the surface structure. In modern MBE systems, several additional surface monitoring techniques are included.

They are: Auger electron spectroscopy (AES), Secondary Ion Mass Spectroscopy (SIMS), X-ray Photon Spectroscopy (XPS), Ultraviolet Photoelectron Spectroscopy (UPS) and Scanning Electron Microscopy (SEM).

AES is used for determining the chemical composition of the growing layer and to determine the bulk chemical composition of the grown structures in terms of depth profiling. SIMS is used for determining the chemical composition of the surface atomic layers and it has high mass resolution. XPS and UPS are used for studying the electronic structure or the energy band distribution at the hetero interfaces. SEM is used for the display of the structure of the growing film or the substrate.

The present day MBE techniques use both Physical Deposition Techniques (PDT) and Chemical deposition techniques (CDT). In PDT, the source material is vaporized at very high temperatures and is transported towards the substrate through a reactor, which is maintained at high vacuum, in the form of vapor without any chemical change. In CDT, the volatile source material is initially produced inside or outside the reactor and is allowed to pass through the reactor to the substrate in the form of vapor. The constituents of the vapor undergo chemical reaction to produce the reactants that aid in the film growth.

2.2 Group III-Nitrides

"Nitrides" is the collective term used for a group of extremely interesting compound semiconductor materials containing *N* such as *InN*, *GaN*, *AlN* and their associated compounds. These compounds are receiving considerable attention because of their opto-electronic application spanning the entire visible spectrum because these materials and

their alloys have energy band gaps covering the range of 1.9-6.2eV, suitable for band-to-band light generation with colors ranging from red to ultraviolet wavelengths [2].

Group III nitrides occur in both zinc blende and wurzitic structure. The wurzitic structure is the most common in *GaN* and its related compounds [2]. The research on group III-nitrides is mainly concerned with the aspects such as achieving cubic β -*GaN*, using usual techniques to grow *GaN* at low temperatures, applying *AlN* buffer layer between the substrate and the film, and using electron beams to achieve *p*-type material. A suitable high quality lattice matched substrate is difficult to obtain in the case of β -cubic *GaN*.

Sapphire substrates are used for the growth of *GaN* in spite of the lattice mismatch between the epilayer and the substrate. The grown layers usually show *n*-type conductivity even though they are not intentionally doped. The donors are probably the residual oxygen or nitrogen vacancies. Use of buffer layers between the epilayer and the substrate helps to improve the surface morphology. *AlN* is the commonly used buffer layer. Use of *GaN* buffer layers instead of *AlN* results in higher quality films [38].

Cheng *et. al.* [39] demonstrated the growth of *GaN* films on *GaAs* surfaces using modified MBE method in which the active nitrogen was supplied from an RF activated plasma source. The *GaN* films grown on (001), (111) A and (111) B *GaAs* substrates at 700 ^{o}C and under similar conditions were compared. Using photoluminescence (PL) spectra it was shown that the best optimum growth was obtained on (111) B *GaAs*. Paisley *et. al.* [40] demonstrated the growth of cubic *GaN* on *Si* by modified MBE. A standard effusive cell was used for *Ga* and a microwave glow discharge was used to activate nitrogen prior to deposition. The grown films were analyzed using Auger

Electron Spectroscopy and Transmission Electron Spectroscopy and were found to be nominally stoichiometric and zinc blende crystal.

Lie *et. al.* [41] studied the epitaxial growth of zinc blende and wurzitic *GaN* films on silicon substrate by Electron Cyclotron Resonance (ECR) assisted MBE, using a two-step process. Initially a *GaN* buffer layer was deposited at low temperature followed by the growth of thicker layers of *GaN* at higher temperature. *GaN* films were found to have either zinc blende or wurzitic structure depending on the single crystalline or polycrystalline buffer layers used, respectively. The growth of *GaN* by ECR assisted MBE was studied by many researchers [42, 43, 44, 45, 46]. Molnar *et. al.* [44] studied the importance of ionic species in the growth of *GaN* by ECR. The ion bombardment was found to have a profound effect on the kinetics of the growth. A transition of film growth from island to three-dimensional mode takes place by varying the microwave power in the ECR's discharge source.

The growth of *GaN* by MBE with radio frequency (RF) nitrogen plasma was studied by [47, 48, 49]. Kubo *et. al.* [47] investigated the growth of homoepitaxial growth of *GaN* thin layer on MOCVD grown *GaN* substrate. It was shown that the homoepitaxial *GaN* had higher crystalline quality by the surface and optical measurements that were made on the sample. It was proposed that the problems of hetero interface between *GaN* and sapphire would be improved by homo epitaxial growth. High quality growth of *AlN* layers on *Si* substrates by Plasma assisted MBE was studied by Sanchez-Garcia *et. al.* [48]. The growth conditions were optimized in order to obtain *AlN* as buffer layers in *GaN* film growth. It was shown that the best films were obtained at substrate temperature greater than 900 ^{o}C and the V/III flux ratios close to stoichiometric values.

High quality *GaN* and *AlN* growth by gas source MBE using ammonia as the nitrogen source was reported by Yang *et. al.* [50] in 1995. The growth rate as high as 1$\mu m/hr.$, the highest ever proposed in gas source MBE was achieved. The low temperature photoluminescence of as-grown materials was dominated by band edge emissions, which indicated the high quality of the materials. Ammonia has been used for the growth of *GaN* by MBE on sapphire substrates by Grandjean *et. al.* [51]. Their experiments were performed, by varying the V/III ratios in the range of 1 - 4. It was found that the increase in V/III ratio improves the material properties, both in terms of optoelectronic and structural quality.

Growth Kinetics of group III nitrides using modified MBE was studied by Foxon *et. al.* [52]. A fixed *Ga* arrival rate of $3\times10^4 atoms/cm^2s$ and constant substrate temperature of 600 ^oC were used in their experiments to grow *GaN* films. The final thickness of the film measured by optical interference method was used to deduce the average growth rate. The growth rate was found to increase with optical emission detector output and saturate above 0.7 values, whereas the *Ga* droplet density formed during the growth showed the reverse characteristic. The film growth under *N*- rich condition in the temperature range of 400-700 ^oC was also studied and it was observed that there was no change in the growth rate.

The dependence of growth rate on temperatures and V/III ratio during *GaN* MBE was studied by Alexeev *et. al.* [53]. The samples were observed through optical reflectivity measurements. It was found that the *GaN* desorption becomes observable at temperature above 800 ^oC which directly relates to reduction in growth rate observed. Desorption was found to be independent of V/III ratio within *N*-rich conditions. Growth

rate reduction of *GaN* due to the surface accumulation of *Ga* was studied by Crawford *et. al.* [54]. It was observed that at high temperatures, the growth rate decreases due to *Ga* desorption and decomposition of *GaN*. At low temperature, the *N* incorporation efficiency was the rate limiting process.

Zsebok *et. al.* [55] studied the surface morphology of the *GaN* as a function of *N/Ga* ratio grown on *GaN* by MBE. The different samples grown under *N*-rich, *Ga*-rich and stoichiometric conditions were analyzed through the SEM. It was concluded that the defect formation at the hetero-interface depends on the *N/Ga* flux ratio. Smith *et. al.* [56] studied the surface reconstruction using the RHEED measurement. It was shown that the smooth (streaky pattern) to rough (spotty pattern) transition of the surface occurs at low *Ga/N* flux ratio.

Many researchers [57, 58, 59, 60] studied the structural and electronic properties of group III nitrides. The optical properties of the crystal depend on the band structure, confined states of energy levels, polarization defects, lattice mismatch between the active layer and the substrate, dopants and defects in the active layer [38, 60, 61]. Higher bandgap enables the material to withstand higher temperatures due to low intrinsic carrier concentrations. The localized energy states confine the carriers to particular energy levels, increasing the intensity of the light. Lattice mismatch introduces strain in the active layer, which leads to changes in the optical property of the material due to lattice constant and hence bandgap energy changes. Dopants and defects act like a recombination center and results in non-radiative recombination of carriers, which in turn, reduces the intensity of the light.

2.3 *InGaN*

GaN does not emit a strong band-to-band emission at room temperature. The non availability of proper substrate (lattice matched) and the difficulty of *p*-type doping of *GaN* paved way for the alloys and hetero structures involving *In* and *Al*. Indium is added to *GaN* to obtain strong band-to-band emission, as *In* introduces deep localized energy states in the bandgap. The *In* content in the *InGaN* can be changed to realize the strong band-to-band emission from green to UV range [62]. Matsuko [63] observed the dependence of the absorption coefficient on the photon energy of *InGaN* epitaxial layer grown at 500 ^{o}C. The plot of absorption co-efficient squared vs. the photon energy in each of the epitaxial layer is linear in the high-energy regime. From their observation *InGaN* has been concluded to have direct band gap as *InN* and *GaN*.

Recently, *InGaN* has become the most promising material for achieving good electrical and optical characteristics from the LEDs [38, 60, 61, 62, 64]. Several researchers have reported growth methods of realizing high quality *InGaN* [31, 32, 65, 66]. Bottcher *et. al.* [67] studied the incorporation behavior of *In* during MBE growth of *InGaN*. The experiments were carried out by varying the *In/Ga* flux ratios and with different film thickness. The samples were analyzed using energy dispersive X-ray microanalysis, high resolution X-ray diffraction and photoluminescence spectroscopy. It was found that *In* incorporation was strongly affected by the *Ga* and *N* fluxes and was limited by excess of nitrogen compared to gallium. It was also found that *In* composition was strongly dependent on the thickness of $In_XGa_{1-X}N$ film.

Okamoto *et. al.* [68] investigated the effects of atomic hydrogen irradiation on the *In* incorporation in *InGaN* films grown by RF plasma assisted MBE growth. The

experiments were carried out for varying substrate temperature and H_2 flow rate, while *N*, *Ga* and *In* flux were kept constant. It was found that the atomic hydrogen irradiation increased the *In* incorporation as the samples grown with *H* had higher *In* content compared to samples without *H* in the substrate temperature range of 640 – 700 ^oC.

O'Steen *et. al.* [69] also studied the effect of V/III flux ratio and substrate temperature on the *In* incorporation behavior in In_XGa_{1-X} /*GaN* hetero-structure grown by RF plasma assisted MBE. Two sets of super lattices were grown. For the first set, the substrate temperature was held constant and the incident fluxes were varied. For the second set, the fluxes were kept constant and the temperature was varied over the range of 540-670 ^oC. Average alloy composition, *In* loss and *In* incorporation efficiency was observed as a function of V/III flux ratio and substrate temperature. The nominal layer composition of *In*, i.e., x, was 30% in $In_XGa_{1-X}N$. It was found that the results obtained from these experiments were consistent with the *In* loss that arises during the growth from thermally activated surface segregation and surface desorption processes.

In segregation during the growth of *InGaN* by plasma assisted MBE, was found by Chen *et. al.* [31, 70]. The dependence of *In* incorporation on growth temperature and group III/V ratio was reported. It was found that *In* incorporation decreases when the growth temperature was increased and decreases when the group III/V flux ratio was increased under metal rich conditions. *In* incorporation was found to increase with flux ratio under nitrogen rich conditions. The surface morphology was also studied using STM images [31, 70, 71]. It was found that the incorporation decreases with the increase in growth temperature, it decreases with the increase in III/V flux ratio under metal-rich conditions and increases with the flux ratio under nitrogen rich conditions. Indium

surface segregation is caused due to the fact that *InN* bond is weaker than the *GaN* bond [31]. A metal atom forms four bonds with nitrogen atoms in the bulk, whereas on the surface a metal atom forms only one bond with the *N* atom in the *N*-polar *InGaN*. So the *Ga* atoms on the surface switch sites with *In* atoms in the bulk as it is energetically favorable for them.

Growth of *GaN*, *AlGaN* and *InGaN* for varying growth conditions were reported in [32]. About 40 monolayers of *InGaN* were grown with different fluxes and temperature between 500-700 ^oC. It was found that below 500 ^oC, *Ga* was strongly bonded and displaced *In* atoms. Above 640 ^oC, high quality layers were obtained. When the *Ga* flux was higher than the *In* flux, no *In* was incorporated in the epilayer.

Chen *et. al.* [65] also observed the spontaneous formation of nano structures in *InGaN*. They showed that these structures arise due to the strain in the surface layers and the relative weakness of *In - N* bond compared to the *Ga-N* bond.

2.4 Doping

The column II impurities when added to *GaN* can either substitute for *Ga* to form single acceptors or for *N* to form deeper triple acceptors. In order to make electronic devices, *pn* junctions are to be formed. *n*-type *GaN* are easily grown but the *p* -doping of *GaN* is difficult. The vapor pressure of *Mg* is very high and it evaporates at around 250 ^oC. The growth of *GaN* by MBE is carried around 750 ^oC, which is much higher than 250 ^oC. This compatibility in temperatures has prompted many research works for the understanding of the incorporation behavior of volatile *Mg* into the epitaxial *GaN*. The thermal activation energy required for ionization of *Mg* is approximately 200*meV*. At

room temperatures, only few percent of acceptor atoms ionize and so to achieve the *p*-type conductivity, large concentration of *Mg* in the layer is required [72].

Amano *et. al.* [73] was the first in obtaining the *p*-type *GaN* films using *Mg* as a dopant. They used MOCVD and post low energy electron beam irradiation (LEEBI) treatment. LEEBI treatment was done after the growth to obtain a low resistivity *p*-type *GaN* film. Saparin *et. al.* [74] investigated LEEBI treatment effects on *Zn* doped *GaN*. But the researches could not succeed in reproducing the doping. Nakamura *et. al.* [75] were the one who found that the *p*-type *GaN* with low resistivity can be obtained by thermal annealing of the MBE grown *GaN* crystals.

The incorporation behavior of *Mg* in *GaN* was studied by [33, 35, 72, 76]. Guha *et. al.* [33] worked on the samples that were grown by MBE using RF source for nitrogen. Infrared pyrometry and SIMS were used to measure the substrate temperature and the *Mg* concentrations, respectively. Experiments were carried out in two sets. In the first set, the temperature was kept constant at 750 ^{o}C and the *Mg* fluxes were varied in the range of 0.04-4 *ML/s*. The other set of experiments were carried out with constant *Mg* flux and varying temperature. It was observed that the *Mg* incorporation is invariant to the arriving *Mg* flux and is strongly dependent on the growth temperature. As the temperature was increased the incorporation of *Mg* decreased.

Two models were suggested to explain the incorporation of *Mg*. In the first model [35, 77, 78, 79], it was suggested that there is a surface accumulation layer with dopant incorporation driven by segregation effects. The other model [80] assumed the presence of finite concentration of *Mg* sites in the growing surface. Cheng *et. al.* [36] studied the mechanism of *Mg* incorporation by AES, SIMS and Hall Effect measurements. It was

shown that *Mg* is uniformly distributed in the bulk and saturates at a concentration of $(2-3)\times 10^{19}\,cm^{-3}$. The concentration of *Mg* was found to decrease from its surface value to its bulk value over depth of approximately 10*nm*, which confirmed that the *Mg* segregates to the surface.

A series of *Mg* step doped epitaxial *GaN* layers were grown by Ptak *et. al.* [72] and the incorporation was studied for (0001) or *Ga* Polarity and $(000\bar{1})$ or *N* polarity. SIMS was used to determine the *Mg* concentration. It was found that *Mg* incorporation depends on polarity and the measurements also supported the surface accumulation of *Mg* during growth. *Mg* incorporation was found to increase in the presence of atomic hydrogen. Myers *et. al.* [76] studied the doping of *GaN* with *Mg* and *Be*. It was also observed that the *Mg* incorporation is dependant on the polarity and substrate temperature. *Mg* incorporation at higher *Mg* flux and higher temperature was found to be approximately twenty to thirty times less in *N*-polar *GaN* while compared to *Ga*-polar *GaN*. It was also shown that the *Be* incorporation in *GaN* by RF plasma MBE is much better than *Mg* doping and is also significantly less dependant on growth conditions.

Cheng *et. al.* [35] studied *Mg–GaN* growth by MBE on *GaAs* substrates. The growth rates of the samples were 0.3 *μm/hr*. The dip in the *Mg* concentration close to the substrate epilayer interface was shown in the SIMS profile and was in close agreement to the work reported in Ref. [81]. In this model, it was assumed that the *Mg* incorporation was from a finite surface concentration and was concluded that high doping density was obtained initially by increasing the *Mg* flux but then it was saturated as the *Mg* surface concentration reached a finite value. Foxon *et. al.* [77] supported the incorporation of *Mg* from a surface concentration maintained during the growth by incident flux.

The effect of growth temperature on *Mg* doped *GaN* was reported in Ref. [34, 82]. Experiments reported in Ref. [34] were carried out in nitrogen rich condition with nitrogen flux of ~ $8.3\times10^{14}\,atoms/cm^2s$. *Ga* flux was maintained at ~ $1.1\times10^{14}\,atoms/cm^2s$, and the flux ratio were as follows: $\frac{J_{Ga}}{J_{Mg}}$~2 and $\frac{J_{Ga}}{J_N}$~0.13. SEM micrographs and AFM were used to study the surface morphology and the grain size as a function of substrate temperature. It was shown that at higher temperature, *Mg* doping promotes diffusion of *Ga* adatoms and enhances the layer-by-layer growth of *GaN.*

Myoung *et. al.* [82] compared the PL spectra of *Mg*-doped *GaN* films grown at two different temperatures. It was found that the films grown at high temperature had good crystalline quality and smooth surface while the films grown at low temperature had poor crystalline quality and rough surface.

The changes in the growth behavior of *GaN* due to the presence of *Mg* as a surfactant were studied by Mulo *et. al.* [83]. It was shown that the growth rate could be increased by 50% depending on the amount of *Mg* and III/V ratio. Daudin *et. al.* [84] found that *Mg* induces drastic changes in the surface diffusion and/or the residence time of both *N* and *Ga*. It was also found that in the nitrogen limited regime, *Mg* increases the amount of *N* available for the growth, due to the desorption rate of *N* atoms. In the *Ga* limited regime more *Ga* is available under fixed *Ga* flux value and the growth rate is increased.

Liliental-Weber *et. al.* [85] accomplished the doping of *GaN* by *Si* and *Mg* incorporation during the film growth. It was found that the post growth treatment is not equired for the *Mg*-doped *GaN* films grown by MBE for electrically activating the dopant. Ng *et. al.* [86] observed the resistivity of *Mg* doped *GaN* films as a function of

the *Mg* cell temperature. It was shown that at low temperatures, the incorporated *Mg* was not sufficient to compensate for the native defects. Increasing the *Mg* flux by four orders showed only an order of magnitude change in the hole carrier concentration of the epilayer. This behavior is explained based on inefficient incorporation of *Mg* due to the high vapor pressure of *Mg* [87]. The *Mg* concentration in the sample was measured using SIMS. The distribution of *Mg* in the epilayer was found to be homogeneous, but there was an accumulation of *Mg* close to the *GaN* and substrate interface. The accumulation of *Mg* was explained due to increased density of structural defects due to lattice mismatch at the interface.

Moustakas *et. al.* [46] worked on the growth and doping of *GaN* films and supported that *p*-type doping of *GaN* films grown by ECR assisted MBE can be obtained without any post growth annealing treatment. The hole carrier concentration at 300 K was found to be between $10^{18} - 10^{19} cm^{-3}$.

2.5 Models

The nature of the growth mechanism in lattice matched III-V compounds grown by MBE were identified for the first time by Madhukar *et. al.* [23]. Monte Carlo simulations were carried out for different *Ga* flux values and substrate temperatures, including additional pathways for arsenic dissociation reaction for GaAs MBE growth. It was shown that the basic nature of growth mechanism remains the same, but the quantitative behavior of specific consequences changes with the growth conditions. The quality of the interface for (100) growth of III-V semiconductor structures was controlled by the cation surface kinetics. Singh *et. al.* [24] studied the role of resonant Laser

enhanced surface kinetics in the MBE growth of compound semiconductors through Monte Carlo simulations.

A quasi-thermodynamic model was developed by Karpov *et. al.* [25] accounting for the kinetics of molecular nitrogen evaporation during the growth simulation of binary and ternary group III-nitrides. The growth processes for the binary nitrides were studied by analyzing the composition of the desorbed vapor species that were influencing the native defect formation in group III-nitrides. The specific features for this growth processes were analyzed. The approach was extended to study the growth of ternary nitrides. Two-drop behavior was found from the plot of growth rate of ternary nitrides and temperature.

A theoretical model [26] was proposed for the analysis of group III-nitrides, which accounts for a physisorption precursor of molecular nitrogen. The high thermal stability of nitrides were explained in relation with the desorption kinetics. The model was quasi thermo dynamic and the conditions of surface liquid formation of nitrides during growth were developed. A theoretical model to study the kinetics of surface processes during the *GaN* growth by MBE with ammonia was proposed by Karpov *et. al.* [27]. Desorption of *Ga* from the surface was considered as the first order reaction. Desorption of nitrogen involving in the association of nitrogen atoms was considered to be the second order reaction. The theoretical results were compared with the experimental results. The temperature dependence of the growth rate was shown to be of bell shaped.

Held *et. al.* [28] developed a rate equation model for *GaN* growth in the temperature regime where the surface morphology remains constant and the decomposition can be neglected. The adsorption of *Ga* on *GaN* $(000\bar{1})$ was studied by exposing the surface to incident *Ga* flux and the desorbing *Ga* flux versus time was measured. Desorption Mass

Spectroscopy was used to study the surface processes. It was shown that the growth could be modeled by the set of rate equations with some assumptions. Fu *et. al.* [36] proposed a rate equation approach for *GaN* growth in order to capture the essence of various experimental data in terms of physical model. All surface processes were assumed to be Arrhenius type. It was shown that the incorporation of *Ga* increases with increasing NH_3 overpressure, saturates at maximum *Ga* flux rate and attains a peak at 820 ^oC.

Also a rate equation model for the *GaN* MBE growth using ECR nitrogen plasma was developed by Fu *et. al.* [29]. The model was similar to the one proposed in Ref. [36]. The unknown model parameters were found by fitting the results from simulation to the experimental values. It was found that as the ECR power was increased, the flux of the by-products were also increased which in turn resulted in the increase of *Ga* incorporation and saturated at a maximum rate. Sipe *et. al.* [30] modeled the *GaN* growth by MBE in the presence of low *Mg* flux using a set of rate equations. *Ga* limited and low – high nitrogen limited regimes were considered and it was assumed that *Mg* induces the incorporation of *Ga*. It was also assumed that the incorporation rate depends on the size of *Ga* cluster. It was shown that the exchange reaction between *Ga* and *Mg* aids in faster growth rate and the *Ga* cluster size dependence of growth rate results in non-monotonic behavior with Ga flux.

2.6 Devices

III-N devices have wide range of commercial applications including high-density optical data storage, full color displays, signal and automotive lighting, solar blind detectors, biological monitoring, high power electronics and underwater communication

[2]. In order to select a material for high power applications the characters that are to be noted are the power losses, switching losses in the high frequency and the critical breakdown field.

GaN exhibits Negative Differential resistance due to various effects that are reported in Ref. [3]. The device studies reported in Ref. [4, 5] have shown the possibility of realizing the NDR diodes. Pavlidis [3] has reviewed the transport characteristics of III-V nitrides and the technology of fabricating such two terminal NDR III-V diodes.

Paul *et. al.* [6] worked on several wide band gap compound semiconductors for superior high voltage unipolar power devices. It was shown that besides *SiC* and diamonds, the materials like *AlN*, *GaN* and *InN* and the intermetallics like $Ga_XIn_{1-X}N$ offers higher magnitude of on- resistance and potential for the operation of devices in higher temperatures. Khan *et. al.* [7] described the current/voltage characteristic collapse in the *AlGaN/GaN* heterostructure insulated gate field effect transistors, that were grown on sapphire substrates, during the high drain bias. They have shown that the devices exhibit both the low and high resistances before and after the application of high drain voltages.

Nichia chemical Industry introduced the high brightness blue LEDs based on *GaN* in 1994 [8]. The diodes are 100 times brighter than the *SiC* blue LEDs. Molnar *et. al.* [9] reported the growth of *p-n* homojuncion LEDs using the Electron Cyclotron Resonance assisted Molecular Beam Epitaxy. The use of ECR technique is to reduce the hydrogen incorporation during the film growth. It was found that these devices emit light in the blue - violet spectrum and they do not require post-annealing treatment for efficient operation in contrast to the similar devices grown by MOCVD.

InGaN can be used in fabricating blue, green, amber, violet and red LEDs. Impurity doping in *InGaN* was performed in order to obtain blue emission spectra. By increasing the indium mole fraction in the active layer, LEDs of 2 cd brightness can be obtained. *InGaN/AlGaN* blue, green LED traffic lights are used in Japan, which consumes only twelve percent of the power when compared to the incandescent traffic lights. III-Nitride devices have a longer lifetime in the order of thousands of hours [10].

Red *InGaN* LEDs with the emission wavelength of 675 *nm* were fabricated by Nakamura *et. al.* [10]. In spite of large thread dislocations (TDs) introduced by *GaN* and sapphire mismatch, *InGaN* based LEDs have efficiency higher than that of conventional III -V compound semiconductors. Experiments were carried out to study the emission mechanism of *GaN* and *InGaN* quantum wells (QWs) by comparing their optical properties as a function of TD density. It was found that the net volume of the light emitting area is reduced by TDs. This negative impact is less effective in *InGaN* QWs where carriers are localized at certain potential. The localized states of an *InGaN* layer play a key role in the high efficiency of LEDs. When electrons and holes are injected into the active layer of LEDs, the carriers are captured by localized energy states before they are captured by the non-radiative recombination centers. Localized excitons with high binding energy are formed and they recombine radiatively.

Mukai *et. al.* [11] fabricated *InGaN* blue LEDs on Epitaxially Laterally Over Grown (ELOG) *GaN* substrates and observed blue shift with increasing forward current. *InGaN* single quantum well blue and green LEDs have a distinct mechanism of blue shift emission energy. Azuhata *et. al.* [12] and Takashi *et. al.* [64] investigated the mechanism that leads to this phenomena and concluded that it is due to the existence of tail energy

states in band edges of *InGaN*.

Nakamura *et. al.* [13] was the first to develop the blue *InGaN/AlGaN* double hetero structures LEDs. Heterosturcture blue, green, amber and violet LEDs were fabricated by many researchers [14, 15, 16, 18, 13]. *GaN* homojunction *p-i-n* photodiode was compared with *AlGaN/GaN* hetero junction *p-i-n* detector and was found that the peaked response exhibited by homo junction near the band edge was absent in the hetero junction [19]. The degradation of blue *AlGaN/InGaN/GaN* LEDs subjected to the high electrical stress was studied by Daniel *et. al.* [17]. It was shown that *GaN* based LEDs are susceptible to electro migration failure under high current pulses.

The fabrication of *GaN* based blue laser diodes have made a revolutionary effect in the production of extremely high-density optical storage systems. *GaN* injection laser was first fabricated by Nakamura *et. al.* [63]. The device consisted of a *p-i-n* junction with multiple quantum wells and with *InGaN* in *i*–region. This transistor comprises of a narrower bandgap base that is made of p-type 6*H SiC*. The normal *Si* transistor needs cooling fins to dissipate the heat generated while operating in high power. But the *GaN/SiC* HBT can operate at elevated temperatures without any cooling means. These devices have excellent inherent internal dissipation of heat.

GaN doped with erbium and oxygen is used for an electrically pumped $1.54\mu m$ laser in optical fiber communication [63]. They are very highly efficient than the narrower bandgap semiconductors. Hot electrons induced luminescence is found to be very efficient at room temperature in *GaN* doped with *Er*, *O*. Nakamura *et. al.* [20] fabricated *InGaN* multi quantum well structure Laser diodes. It was shown that the cleaved mirror facet showed a high output power under room temperature. The lifetime of the LDs at

constant output power of $5mW$ was found to be 160 $hr.$ under CW operation at 50 ^{o}C ambient temperature.

CHAPTER 3

THEORETICAL FORMULATION

3.1 Surface Processes

The MBE growth simulation of *InGaN* on wurtzitic *GaN* substrate oriented along [0001] and *Mg* doping of wurtzitic *GaN* were considered. The dynamic processes occurring on a surface riding physisorbed material layer (PM) and the surface of the crystalline epilayer play a crucial role in the growth and composition of compound semiconductors. The atoms or molecules of this layer are physisorbed on to the surface by Vander Waals type of binding, i.e., weakly bonded to the surface.

Several dynamic processes such as the adsorption of atom onto the crystal, the evaporation of atom out of it and the segregation of atoms from the bulk into the PM layer are considered for the PM layer. These processes are assumed to be Arrhenius type and are given by:

$$\tau_i = \tau_{o,i,e} e^{\frac{E_i}{kT}} \tag{1}$$

where $\tau_{o,i,e}$ represents the time constant for the process i, E_i is the activation energy, k is the Boltzmann constant and T is the temperature in Kelvin.

The surface dynamic processes included for the epilayer are adsorption, evaporation, interlayer migration, intralayer migration and segregation. A schematic picture of these processes is shown in Figure 1 for *InGaN* and Figure 2 for *Mg-GaN*. Arrhenius type rate

equations are assumed for the rate of evaporation and migration of atoms, and are given by:

$$R = R_o e^{\frac{-E_{act}}{kT}} \tag{2}$$

where R_o is the frequency prefactor, E_{act} is the activation energy, k is the Boltzmann constant and T is the temperature in Kelvin.

3.2 Time Evolution Equations

3.2.1 *InGaN* Growth

The time evolution of the growing epilayer is described through the change of macro variables such as coverages of individual species resulting from the surface processes. The macro variables of growth are normalized with respect to the maximum number of possible atoms in the layer, and therefore have values between 0 and 1. Coverage is 1 when the layer is full and 0 when the layer is empty.

The layer coverages of *Ga*, *N*, and *In* in their respective layers are the macro variables describing the growth and are denoted as:

$C_{Ga}(2n)$: layer coverage of *Ga* in the $2n^{th}$ layer,

$C_N(2n+1)$: layer coverage of *N* in the $2n+1^{th}$ layer,

$C_{In}(2n)$: layer coverage of *In* in the $2n^{th}$ layer,

C_{Ga}^{PM}, C_N^{PM} and C_{In}^{PM} :PM layer coverage of *Ga*, *N* and *In* respectively. (3)

where n is the layer index, with the Ga and In belonging to even numbered layers, and the N belonging to the odd numbered layers. Note that the coverages can have values

between 0 and 1, depending on how full a layer is.

The time evolution of the layer coverage of *In* in the $2n^{th}$ layer due to the various surface processes is given by:

$$\frac{dC_{In}(2n)}{dt}=\left([C_N(2n-1)-C(2n)]\times\left[J_{In}+\frac{C_{In,phy}}{\tau_{in}^{In}}\right]\right) \quad \text{(A1)}$$

$$+[C_N(2n-1)-C(2n)]\times\left(R_0e^{\frac{E_{d,In}(2n+2)}{kT}}\left(\frac{C_{In}(2n+2)}{C(2n+2)}\right)\right.$$

$$\times[C(2n+2)-C_N(2n+3)]$$

$$\left.+R_0e^{\frac{E_{d,In}(2n-2)}{kT}}\left(\frac{C_{In}(2n-2)}{C(2n-2)}\right)\times[C(2n-2)-C_N(2n-1)]\right) \quad \text{(B1)}$$

$$-R_0e^{\frac{E_{d,In}(2n)}{kT}}\left(\frac{C_{In}(2n)}{C(2n)}\right)\times[C(2n)-C_N(2n+1)]$$

$$\times([C_N(2n+1)-C(2n+2)]+[C_N(2n-3)-C(2n-2)]) \quad \text{(C1)}$$

$$-R_0e^{\frac{E_{e,In}(2n)}{kT}}\left(\frac{C_{In}(2n)}{C(2n)}\right)\times[C(2n)-C_N(2n+1)] \quad \text{(D1)}$$

$$-R_0e^{\frac{E_{s,In}(2n)}{kT}}\left(\frac{C_{In}(2n)}{C(2n)}\right)\times[C(2n)-C_N(2n+1)] \quad \text{(E1) (4)}$$

where the term A1 represents the increase in $C_{In}(2n)$, resulting from adsorption of *In* from the incoming flux. The rate of adsorption is the product of the available sites for *In* incorporation on the surface, $[C_N(2n-1)-C(2n)]$, and the fluxes of *In*, J_{In} from the molecular beam and $\frac{C_{In,phy}S_1}{\tau_{in}^{In}}$ from the PM layer. The sticking coefficient of *In* is taken

as unity. The term B1 describes the increase in $C_{In}(2n)$ resulting from migration of *In* into the $2n^{th}$ layer from all the adjacent layers, i.e., $(2n+2)$ and $(2n-2)$. $[C(2n-2)-C_N(2n-1)]$ is the fraction of available sites for *In* in the $2n^{th}$ layer. *In* and *Ga* are the two possible elements in the cation sub-lattice. The total coverage of a cation layer, $C(2n+2)$, is given by:

$$C(2n+2)=C_{Ga}(2n+2)+C_{In}(2n+2) \tag{5}$$

The fraction $\frac{C_{In}(2n+2)}{C(2n+2)}$ is used to include only the *In* portion of all the cations in the layer for migration. The activation energy for *In* diffusion in the $2n\text{-}2^{th}$ layer depends on the coverage of the layer and is given as:

$$E_{d,In}(2n-2)=E_{d,In,iso}+6E_{In,In}C_{In}(2n-2)+6E_{Ga,In}C_{Ga}(2n-2) \tag{6}$$

where, $E_{d,iso}$ is the activation energy of isolated atoms, and the second neighbor atom-atom pair interaction energies, $E_{Ga,In}$ and $E_{In,In}$, with a factor of six for the maximum possible number of neighboring atoms. Thus, when the coverage is very small, $E_{d,In}(2n-2)$ equals $E_{d,In,iso}$. $[C_N(2n)-C(2n+1)]$ is the portion of the n^{th} layer available for diffusion of *Ga/In* from the neighboring layers. Term C1 represents the migration process opposite to that represented by the term B1. The terms D1 and E1 in Equation (4) describes the decrease in $C_{In}(2n)$ resulting from the evaporation and segregation of *In* atoms, respectively, from the $2n^{th}$ layer. $\frac{C_{In}(2n)}{C(2n)}[C(2n)-C_N(2n+1)]$ represents the fraction of *In* in the $2n^{th}$ exposed layer to the vacuum so that it is available for segregation or evaporation.

The descriptions of the activation energy for evaporation and segregation are similar to that of diffusion given by equation (4), except for the value for the isolated adatom. The equations are

$$E_{e,In}(2n) = E_{e,In,iso} + 6E_{In,In}C_{In}(2n) + 6E_{Ga,In}C_{Ga}(2n) \tag{7}$$

and

$$E_{s,In}(2n) = E_{s,In,iso} + 6E_{In,In}C_{In}(2n) + 6E_{Ga,In}C_{Ga}(2n) \tag{8}$$

for evaporation and segregation, respectively.

The time evolution of the layer coverage of *In* in the PM layer, $\frac{dC_{In}}{dt}$, is given by:

$$\frac{dC_{i,phy}}{dt} = \begin{array}{l} (J_i(1-S_1)) - \frac{C_{i,phy}}{\tau^i_{ev}} - \frac{C_{i,phy}S_1}{\tau^i_{in}} + R_0 e^{\frac{-E_s(2n)}{kT}}\left(\frac{C_{i,phy}(2n)}{C(2n)}\right) \\ \times[C(2n) - C_N(2n+1)] \end{array} \tag{9}$$

where i represents *In* in this case and S_1 is the sum of all crystal sites that are available for the incorporation of species in the appropriate sub-lattice. J_i is the molecular flux of the ith species coming onto the substrate. The first term denotes the increase in PM coverage due to arrival of ith species flux. The second and third term denotes the net loss of PM layer coverage due to evaporation and chemisorption. The last term denotes the gain in the PM layer coverage due to segregation.

A similar equation is written for physisorbed Ga and *N* without the segregation term and the *N* getting incorporated in the anion sub-lattice. As only monolayer coverage of the PM layer is effective in the surface dynamics, the sum of the coverage of *Ga*, *In* and *N* in the PM layer cannot exceed 1. R_0 is the frequency factor and $E_s(2n)$ is the activation energy for the segregation of the ith species from the crystal surface to the PM layer.

Equations similar to 4-9 are written for N and Ga, except that the term E, which represents segregation, is excluded from them.

The time evolution of the layer coverage of Ga in the $2n^{th}$ layer due to the surface processes is given by

$$\frac{dC_{Ga}(2n)}{dt}=\left([C_N(2n-1)-C(2n)]\times\left[J_{Ga}+\frac{C_{Ga,phy}}{\tau_{in}^{Ga}}\right]\right) \quad \text{(A2)}$$

$$+[C_N(2n-1)-C(2n)]\times\left(R_0 e^{\frac{E_{d,Ga}(2n+2)}{kT}}\left(\frac{C_{Ga}(2n+2)}{C(2n+2)}\right)\right.$$

$$\times[C(2n+2)-C_N(2n+3)]$$

$$\left.+R_0 e^{\frac{E_{d,Ga}(2n-2)}{kT}}\left(\frac{C_{Ga}(2n-2)}{C(2n-2)}\right)\times[C(2n-2)-C_N(2n-1)]\right) \quad \text{(B2)}$$

$$-R_0 e^{\frac{E_{d,Ga}(2n)}{kT}}\left(\frac{C_{Ga}(2n)}{C(2n)}\right)\times[C(2n)-C_N(2n+1)]$$

$$\times([C_N(2n+1)-C(2n+2)]+[C_N(2n-3)-C(2n-2)]) \quad \text{(C2)}$$

$$-R_0 e^{\frac{E_{e,Ga}(2n)}{kT}}\left(\frac{C_{Ga}(2n)}{C(2n)}\right)\times[C(2n)-C_N(2n+1)] \quad \text{(D2) (10)}$$

The terms A2, B2, C2 and D2 are similar to A1, B1, C1 and D1 respectively.

The time evolution of layer coverage of N is given by:

$$\frac{dC_N(2n+1)}{dt}=\left([C(2n)-C(2n+1)]\times\left[J_N+\frac{C_{N,phy}}{\tau_{in}^{N}}\right]\right) \quad \text{(A3)}$$

$$+[C(2n)-C(2n+1)]\times\left(R_0 e^{\frac{E_{d,N}(2n+3)}{kT}}\left(\frac{C_N(2n+3)}{C(2n+3)}\right)\right.$$

$$\times[C(2n+3)-C(2n+4)]$$

$$+R_0 e^{\frac{E_{d,N}(2n-1)}{kT}}\left(\frac{C_N(2n-1)}{C(2n-1)}\right)\times[C(2n-1)-C(2n)]\Bigg) \quad \text{(B3)}$$

$$-R_0 e^{\frac{E_{d,N}(2n+1)}{kT}}\left(\frac{C_N(2n+1)}{C(2n+1)}\right)\times[C(2n+1)-C(2n+2)]$$

$$\times([C(2n+2)-C_{Ga}(2n+3)]+[C(2n-2)-C(2n-1)]) \quad \text{(C3)}$$

$$-R_0 e^{\frac{E_{e,N}(2n+1)}{kT}}\left(\frac{C_N(2n+1)}{C(2n+1)}\right)\times[C(2n+1)-C(2n+2)] \quad \text{(D3) (11)}$$

where the terms A3, B3, C3 and D3 are similar to A1,B1,C1 and D1 respectively.

3.2.2 *Mg-GaN* Growth

The model used to describe *Mg-GaN* growth is same as the one used for *InGaN* growth except for the equation representing the activation energy of *Mg* diffusion. All the equations in *InGaN* except equations (7) and (8) are employed in this model with the subscript *In* changed to *Mg*.

The activation energy for *Mg* diffusion in the 2n-2th layer depends on the coverage of the layer and is given as:

$$E_{d,Mg,u}(2n-2)=E_{d,Mg,iso,u}+6E_{Mg,Mg}C_{Mg}(2n-2)+6E_{Ga,Mg}C_{Ga}(2n-2)$$

and

$$E_{d,Mg,d}(2n-2)=E_{d,Mg,iso,d}+6E_{Mg,Mg}C_{Mg}(2n-2)+6E_{Ga,Mg}C_{Ga}(2n-2) \quad (12)$$

where, $E_{d,iso,u}$ is the activation energy of isolated atoms moving upwards and $E_{d,iso,d}$ is the activation energy for atoms moving downwards, and the second neighbor atom-atom pair interaction energies, $E_{Ga,Mg}$ and $E_{Mg,Mg}$, with a factor of six for the maximum possible number of neighboring atoms. Thus, when the coverage is very small,

$E_{d,Mg}(2n-2)$ equals $E_{d,Mg,iso}$. $[C_N(2n)-C(2n+1)]$ is the portion of the nth layer available for diffusion of *Ga*/*Mg* from neighboring layers. The differentiation made here for *Mg* migrating up or down is not done for *In* migration as described in section 3.2.1.

3.3 Computational details and model parameters

Three first order nonlinear differential equations are required for the description of the evolution of each bilayer of *InGaN*/*Mg-GaN* with one equation describing the time evolution of each of the normalized macro-variables. Three additional equations are required for describing the time evolution of the PM layer. For this work, a total of 243 coupled nonlinear first order differential equations are required to solve the simultaneous growth of 80 bilayers and the PM layer.

Fourth order Runge-Kutta method was used to integrate the system of equations with time steps of less than 10^{-6} s to compute the values of each of the macro-variables as a function of time for a growth time of 40 s. Similarly the activation energies for *In*, *Ga* and *N* evaporation process from the PM layer, E_{ev}^{In}, E_{ev}^{Ga} and E_{ev}^{N} respectively for *InGaN* and E_{ev}^{Mg}, E_{ev}^{Ga} and E_{ev}^{N} for *Mg-GaN* are assumed to be linearly dependent on their own coverage in the physisorbed layer [Table 1].

In the case of *InGaN*, in order to make the model simple, the 2nd neighbor interaction energies are kept the same and also the 1st neighbor interaction energy between III-V atoms are kept identical. In *Mg-GaN* the first neighbor interaction energy between *Ga-N* and *Mg-N* are made equal. The first neighbor interaction energy between *Mg-Ga* is made smaller and is equal to the second neighbor interaction energies. The prefactor of time constants for incorporation and evaporation processes are obtained according to the

Arrhenius equation and related to the activation energies. The evaporation, segregation and diffusion processes in the surface of the epilayer are assumed to be thermally activated and are modeled with the frequency factor, R_0 and activation energy. R_0 is linearly dependent on the substrate temperature, and is given by:

$$R_0 = 2.08 \times 10^{10} \times T \tag{13}$$

This is based on the phonon frequency obtained using the equipartition energy principle. The frequency prefactor of diffusion processes are assumed constants. The frequency prefactor for segregation is considered to be linearly dependent on the substrate temperature, and is given by:

$$R_{0,s} = 1.743 \times 10^{10} \times T \tag{14}$$

The segregation process from the PM layer is allowed only for *In* in the *InGaN* and only for *Mg* in *Mg-GaN*. It is noted that $R_{0,s}$ is smaller than the R_0 of evaporation and diffusion. The frequency factors for the other processes are:

$R_0^{d,Ga}$ frequency factor for N for diffusion 4.38×10^7/s

$R_0^{d,N}$ frequency factor for Ga for diffusion 2.4×10^8/s.

$R_0^{d,In}$ and $R_0^{d,Mg}$ frequency factor for In and Mg for diffusion 4.38×10^5/s. (17)

3.4 Conversion among various flux units

The flux rates given in $atoms/cm^2s$ are converted to $\left(\frac{ML}{s}\right)$. The conversion is done by multiplying the flux in $atoms/cm^2s$, with the *area/site* of the wurzitic structure.

$$J\left(\frac{ML}{s}\right) = J\left(\frac{atoms}{cm^2s}\right) \times \frac{\sqrt{3}}{2}a^2, \tag{18}$$

where a is the lattice constant. For GaN $a = 3.189A^{o}$ and hence,

$$J\left(\frac{ML}{s}\right) = 8.8072\times10^{-16}\times J\left(\frac{atoms}{cm^{2}s}\right) \tag{19}$$

For the wurzitic structure c = 5.185 A^{o} and every monolayer is equal to $\frac{c}{2}$ and hence,

$$J\left(\frac{ML}{s}\right) = \frac{J\left(\frac{nm}{\min}\right)}{\frac{c}{2}\left(\frac{nm}{\min}\right)} \tag{20}$$

CHAPTER 4

RESULTS AND DISCUSSIONS

4.1 *InGaN*

The growth conditions for the simulations were obtained from Averbeck *et.al.* [32]. The simulations were performed for two different nitrogen fluxes - 4.7*nm/min* and 12 *nm/min* and for the various temperatures in the range of 500-700 ^oC. The *In* content versus temperature plot shown in Figure 3 is obtained for the J_{Ga}/J_N ratio of 0.5 for various J_{In}/J_{Ga} ratios in the range of 0.33-3.0. The behavior of the plots is within 1% agreement with the plots in Figure 1.a of Ref. [32]. It is found that for a given set of fluxes, below 580 ^oC, the fraction of *In* incorporated in to the layer closely follows the ratio of *In* flux to the total flux, i.e., J_{In}/J_{total}, and the percentage of Indium content in the layer is constant. Above 580 ^oC, the segregation phenomenon begins to dominate the kinetics due to increased thermal energy and hence, *In* content decreases with increasing temperature. Above 640 ^oC, only a trace of *In* is found in the growing layer. The active segregation energy of *In* is found from our simulation to be 2.9 *eV*, which is in close agreement with the segregation energy given in Ref. [32].

The *InN* loss as a function of temperature for various flux conditions is shown in Figure 4. The *InN* loss rate here is computed as the difference between the *In* flux and the incorporation rate of *In* and hence, includes both the loss of *In* due to segregation and the

non-availability of N site. The simulations results show that for Group III rich conditions, the incorporation of Indium is limited by the nitrogen flux independent of the temperature. For N-rich growth conditions, at temperatures below 580 ^oC, the *InN* loss rate is insignificant as there is negligible segregation of *In* atoms due to lack of thermal energy necessary for overcoming the segregation barrier. Above 640 ^oC, the loss rate attains a maximum value of the *In* flux, J_{In}. The results of Figure 3 and Figure 4 are consistent.

Plots of percentage of *Ga* content in the layer as a function of temperature for various fluxes are shown in Figure 5. At lower temperatures the incorporation of *Ga* governed by the ratio of J_{Ga}/J_{total}. At temperature above 640 ^oC the *Ga* content is 100%, as all *In* segregates to the surface. Thus, the results of Figure 3 and Figure 4 are in consistent with that of Figure 5.

Plots of growth rate versus temperature are shown in Figure 6 for various flux conditions. For J_N=4.7 *nm/min* and J_{In} / J_{Ga}=3.2, J_{In} + J_{Ga} = 9.9 *nm/min*., the growth rate was observed to be 3.2 *nm/min* at low temperatures and drops down to 1.6 *nm/min* at high temperatures. For J_N = 4.7*nm/min* and J_{In} / J_{Ga}=1.1, J_{In} + J_{Ga} = 4.9*nm/min*, the growth rate is 2.5 *nm/min* at low temperatures and decreases to 1.6*nm/min*. for high temperatures. At low temperatures, *In* contributes to the growth rate in accordance to the flux ratio of *In* to *Ga*. At high temperatures, *In* segregates and hence the growth rate stays constant, irrespective of the ratio of *In* and *Ga* flux.

4.2 *Mg-GaN*

The initial growth conditions are obtained from Myoung *et. al.* [34]. The flux of nitrogen and flux ratios as given in [34] were $8.3\times10^{14}\, atoms/cm.^2 s.$, $\left(\frac{J_{Ga}}{J_N}\right) \sim 0.13$ and $\left(\frac{J_{Ga}}{J_{Mg}}\right) \sim 2$ respectively. So the simulations are run for different temperatures in the range of 600-700 ^oC and at a particular flux rates of *Mg*, *Ga* and *N*, such as $5.5\times10^{13}\, atoms/cm^2 s$, $1.1\times10^{14}\, atoms/cm^2 s$ and $8.3\times10^{14}\, atoms/cm^2 s$ respectively.

Plot of *Mg* dopant concentration vs. layer number at 600 ^oC for various growth times is shown in Figure 7. For this plot, only layers that are full (i.e., $C_{Mg} + C_{Ga} = 1$) after a particular time are considered. The temperature was kept constant at 600 ^oC. Plots were obtained for various time periods of growth in seconds. The peak value in each plot denotes the maximum surface concentration at that particular layer at a particular time. The values to the left of the peak point represent the bulk concentration and to the right represent the surface concentration. Initially *Mg* concentration at the surface close to the substrate is high and as the epilayers grow the surface concentration of the growing epilayer increases. *Mg* concentration at the surface close to the substrate decreases, which shows that there is a segregation of *Mg* from layer to layer.

Plot of Mg concentration vs. layer number at 680 ^oC for various growth times is shown in Figure 8. Comparing Figures 7 and 8, it is observed that as the temperature increases, more and more *Mg* segregates to the surface and hence the bulk *Mg* concentration decrease with increase in temperature. This is in qualitative agreement with the experimental results in Ref. [34].

Due to computational limitations, it is not possible to simulate growth of films of thickness ½ μm. Thus an extrapolated scheme was adopted which is described below.

A cubic curve fitting is obtained for a plot of particular temperature in order to obtain the maximum *Mg* concentration at various time periods of growth. Using the maximum Mg concentration obtained for various times, the constants a, b and c for the extrapolated equation

$$y_{\max}(t) = a\left(1 - e^{-bt}\right) + c \tag{21}$$

were obtained. Using equation 21, $y_{\max}(t)$ values were obtained for $t = 5$ minutes. The constants for the extrapolated maximum *Mg* surface concentration at various temperatures are listed in Table 2.

The extrapolated plot of maximum *Mg* surface concentration vs. time is shown in Figure 9. The surface concentration increases with time and reaches a constant value, which implies that *Mg* segregates to the surface and saturates at a particular concentration. The result is in close agreement with Figure 1.a in Ref. [35]. The extrapolated *Mg* surface concentration vs. thickness of the crystal from the substrate, for various growth temperatures, is shown in Figure 10. The surface concentration increases from the substrate and reaches a maximum at the surface of the crystal. Also the saturated *Mg* concentration increases with temperature and attains a peak value at 680 ^{o}C. Above 680 ^{o}C, the saturation value starts to decrease.

A plot of minimum and maximum *Mg* concentration vs. temperature is shown in Figure 11. The minimum concentration implies the bulk *Mg* concentration and the maximum concentration implies the surface concentration. The bulk *Mg* concentration is obtained from the plots of dopant concentration vs. layer number for various

temperatures as shown in Figure 7 and 8. The point at which the plots start for various time periods is taken as the minimum bulk *Mg* concentration. At low temperatures the thermally activated segregation energy that aids in layer-to-layer segregation is not dominant. But as the temperature increases, segregation also increases and the surface concentration of *Mg* is maximum at 680 ^oC. Figure 11 is consistent with Figure 10.

When the temperature is raised above 750 ^oC there is a dip in the *Mg* concentration near the surface layer as shown in Figure 11. This region is called as dopant depleted zone. The rate of these migration from one layer to the other depends on the availability of *Mg* in the layers that are exposed to the vapor and the available sites in the layer to which the atoms migrate. For example, considering the n^{th} layer, the ratio of atoms migrating to the n^{th} layer to the atoms moving out of this layer is small. i.e. the rate of migration from the subsurface to the surface layer is larger than the rate of migration of atoms to the surface from the bottom layer. This gives rise to the deficiency of *Mg* atoms near the surface layer. The dip shown in Figure 12 is in good qualitative agreement with the plots in Ref. [33, 34, 82].

CHAPTER 5

CONCLUSIONS AND RECOMMENDATIONS

The growth of *InGaN* and *Mg-GaN* by Molecular Beam Epitaxy is investigated with the rate equation model. The dependences of growth kinetics and *In/Mg* content on the temperature and flux conditions are analyzed using the simulation of the model. In the *InGaN* growth it is observed that the segregation phenomenon plays a major role in the surface kinetics and hence the *In* content of the grown layers. *In* segregation is found to be negligible below 580 ^{o}C. Above 640 ^{o}C, the segregation dominates the kinetics. This temperature dependence is found to be independent of the fluxes. In *Mg-GaN* growth, the phenomenon of segregation is justified with the simulation results and is in excellent agreement with the experimental results. The segregation of *Mg* is found to be dependant on the growth temperature. A dopant depleted zone near the surface is found to be formed during the growth at higher temperature. The observation is in qualitative agreement with the experimental data.

The following issues are recommended for further investigations:

- The dependence of *Mg* incorporation on the incident fluxes can be studied by simulating the model under various incident flux values.
- Theoretical models can be formulated for many experimental models that describe the incorporation behavior of *Mg* in *Mg-GaN*.

Table 1. Parameters, their symbols and values used in the simulation. *X* represents *In* in *InGaN* and *Mg* in *Mg-GaN*

Symbol	Parameter Name	***InGaN*** **(eV)**	***Mg-GaN*** **(eV)**
$E_{X\text{-}X}$	2nd neighbor atom-atom pair interaction energy for *X* cations.	0.08	0.08
$E_{Ga\text{-}Ga}$	2nd neighbor atom-atom pair interaction energy for *Ga*	0.08	2.00
$E_{N\text{-}N}$	2nd neighbor atom-atom pair interaction energy for *N*	0.08	0.08
$E_{Ga\text{-}X}$	1st neighbor atom-atom pair interaction energy for *Ga-X*	0.08	0.08
$E_{Ga\text{-}N}$	1st neighbor atom-atom pair interaction energy for *Ga-N*	2.0	2.0
$E_{X\text{-}N}$	1st neighbor atom-atom pair interaction energy for *X-N*	2.0	2.0
$E_{d,iso,Ga}$	Activation energy for diffusion for isolated *Ga* atom	1.2	1.2
$E_{d,iso,N}$	Activation energy for diffusion for isolated *N* atom	1.2	1.2
$E_{d,iso,X}$	Activation energy for diffusion for isolated *X* cation atom	1.2	$E_{d,iso,u}$= 0.25 $E_{d,iso,d}$= 1.2
$E_{e,iso,Ga}$	Activation energy for evaporation for isolated *Ga* atom	6.24	12.0
$E_{e,iso,N}$	Activation energy for evaporation for isolated *N* atom	6.24	6.24
$E_{e,iso,X}$	Activation energy for evaporation for isolated *X* cation atom	6.24	6.24
$E_{ev,Ga}$	Activation energy for the physisorbed *Ga* evaporation	$0.18 + 0.06C_{Ga,phy}$	$0.18 + 0.06C_{Ga,phy}$
$E_{ev,N}$	Activation energy for the physisorbed *N* evaporation	$0.18 + 0.06C_{N,phy}$	$0.18 + 0.06C_{N,phy}$
$E_{ev,X}$	Activation energy for the physisorbed *X* cation evaporation	$0.18 + 0.06C_{X,phy}$	$0.18 + 0.06\,C_{X,phy}$
$E_{in,Ga}$	Activation energy for the *Ga* incorporation	0.0	0.0
$E_{in,N}$	Activation energy for the *N* incorporation	2.9	2.9
$E_{in,X}$	Activation energy for *X* cation incorporation	$0.5\,C_{X,\,phy}$	$0.5\,C_{X,\,phy}$
$E_{seg,\,X}$	Activation energy for X cation segregation	2.9	2.9

Table 2 Constants for the extrapolated maximum Mg concentration $y_{\max}(t)$ at various temperatures

Temperature (^{o}C)	a	b	c
600	-2.2e-04	4.6e-04	0.0336
625	-8.9e-05	4.8e-04	0.0223
650	-1.5e-03	2.0e-03	0.0511
675	-2.6e-04	8.4e-04	0.0288
680	-3.1e-04	9.0e-04	0.0288
700	-1.2e-03	1.7e-03	0.0511
725	9.3e-05	2.3e-04	0.0105

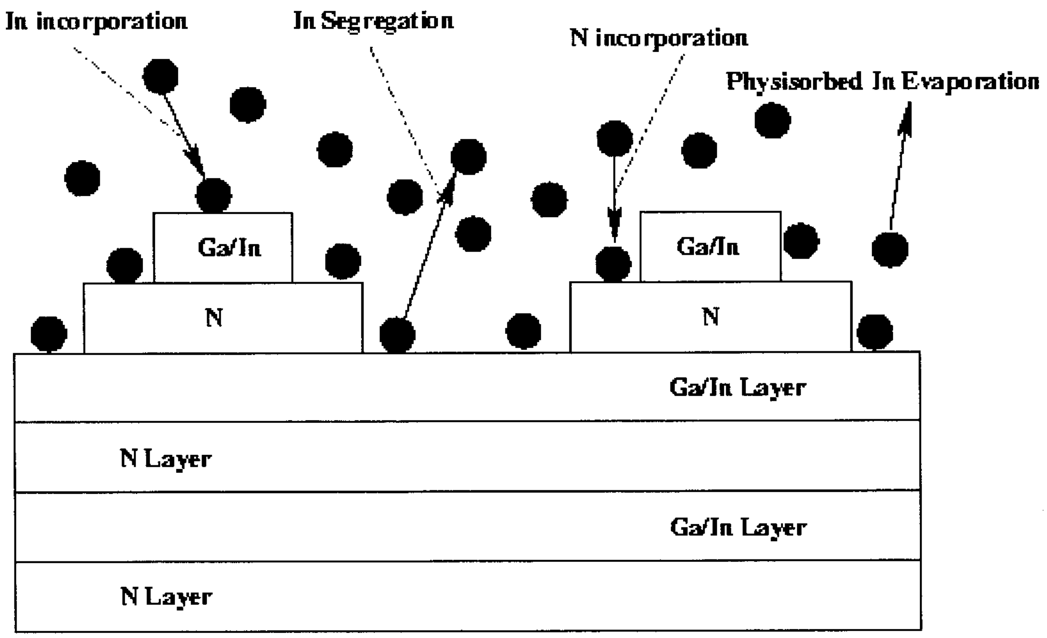

FIGURE 1: A schematic picture of the surface processes in MBE growth of *InGaN*

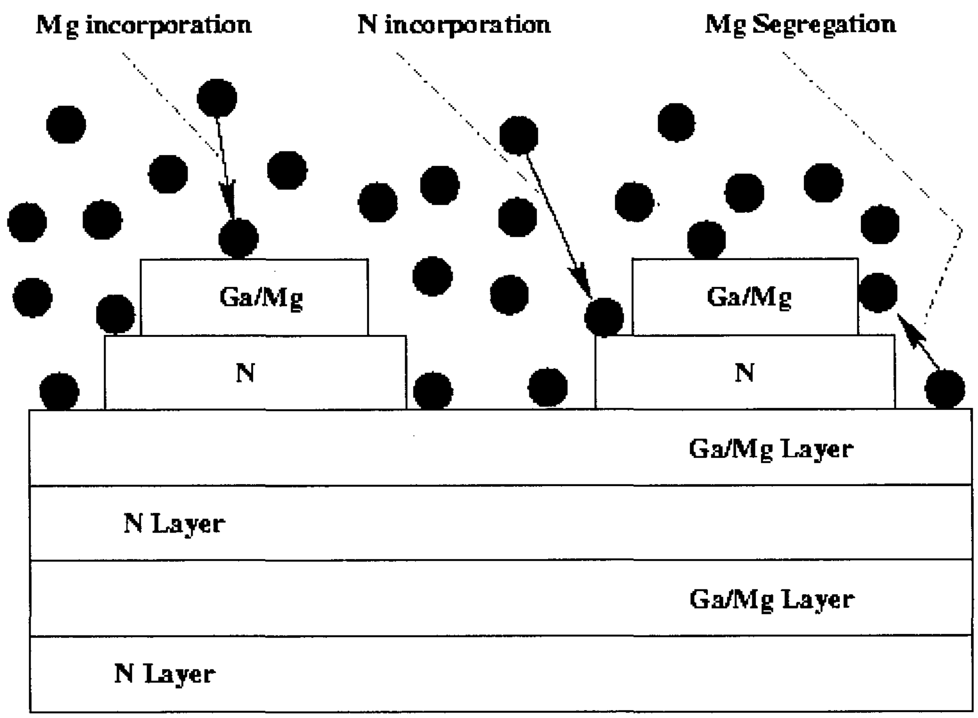

FIGURE 2: A schematic picture of the surface processes in MBE growth of *Mg-GaN*

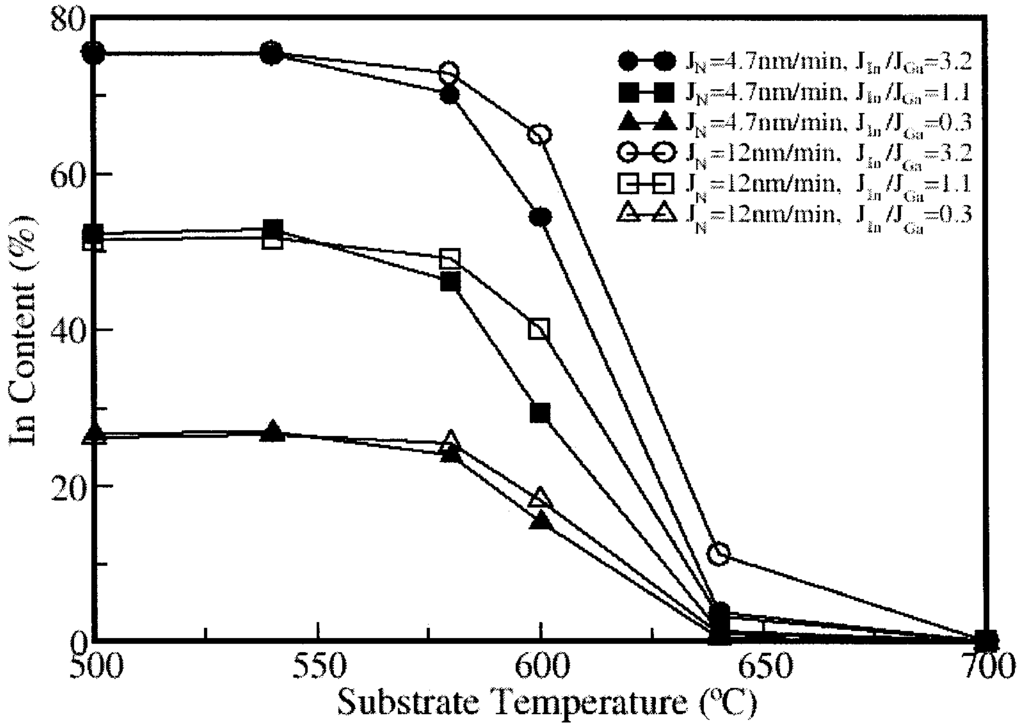

FIGURE 3: Plots of Indium content in percentage vs the substrate temperature for the nitrogen fluxes of 4.7 *nm/min* and 12 *nm/min*, and various ratios of *In* and *Ga* fluxes.

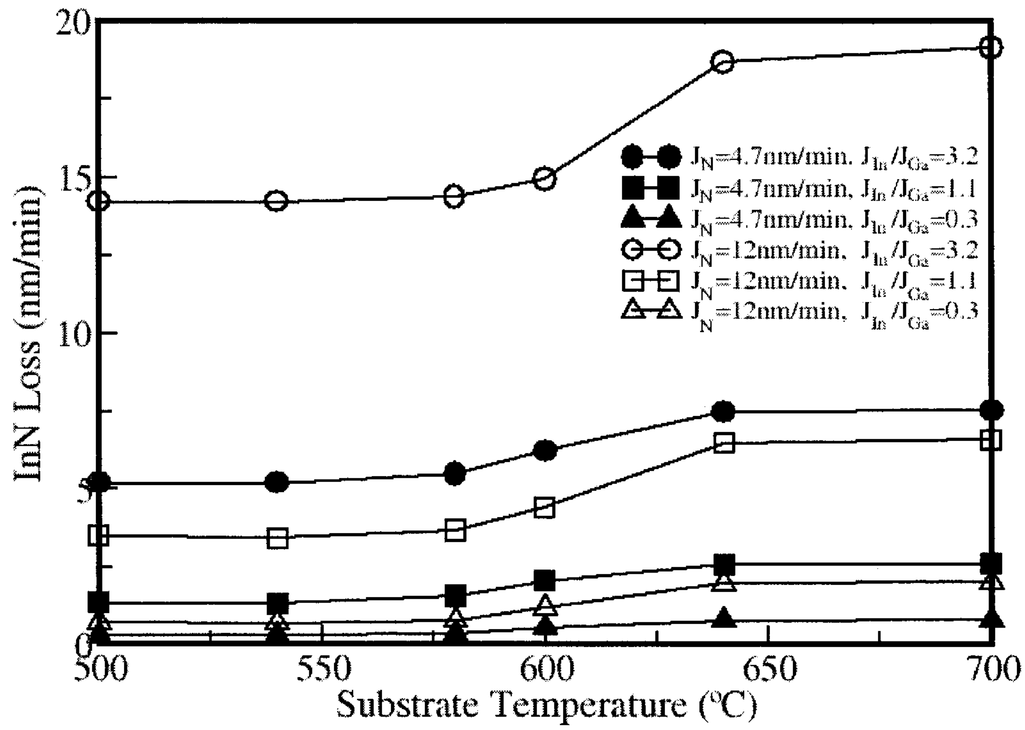

FIGURE 4: Plots of *InN* loss rate vs temperature for the nitrogen fluxes of 4.7 *nm/min* and 12 *nm/min*, and various ratios of *In* and *Ga* fluxes.

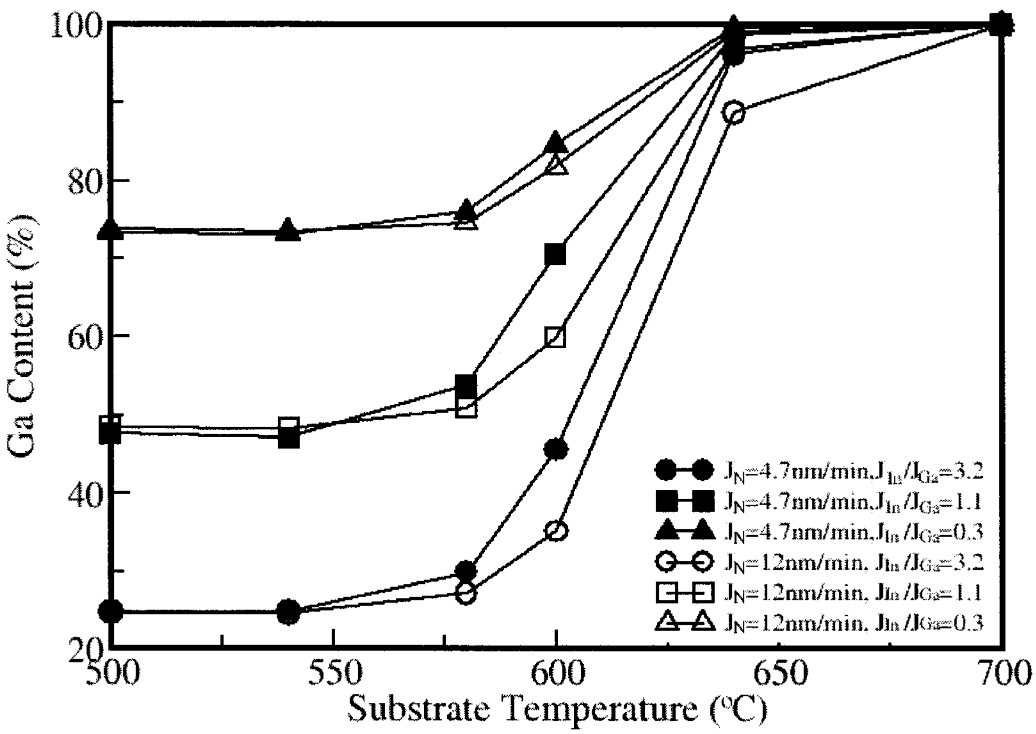

FIGURE 5: Plots of *Ga* content in percentage vs substrate temperature for the nitrogen fluxes of 4.7 *nm/min* and 12 *nm/min*, and various ratios of *In* and *Ga* fluxes.

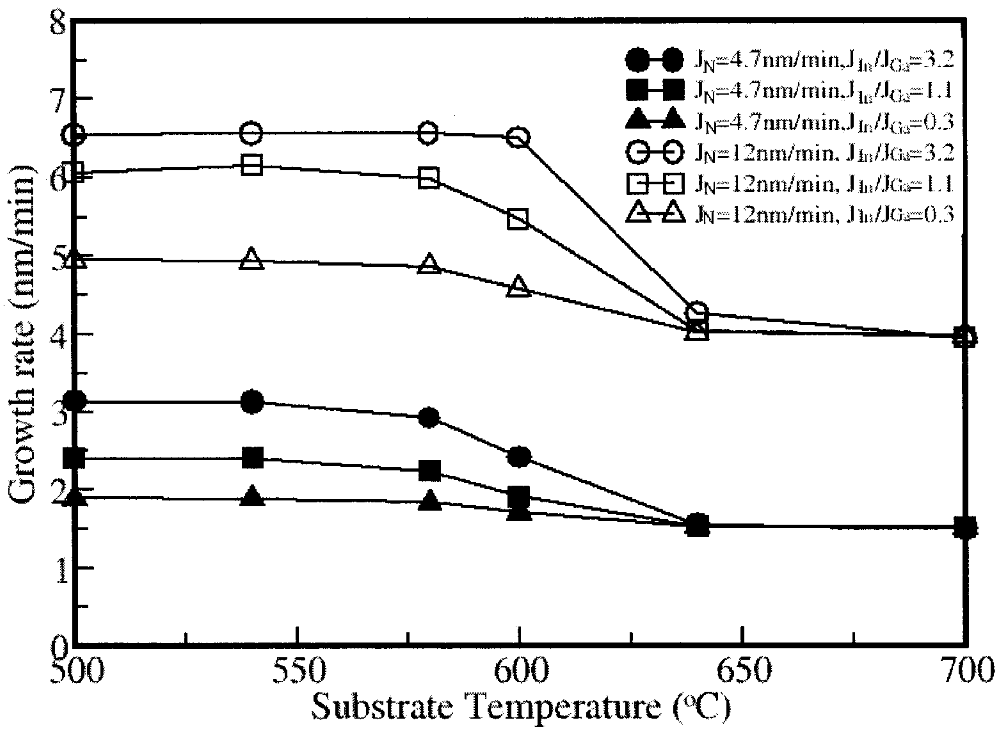

FIGURE 6: Plots of growth rate vs substrate temperature for the nitrogen fluxes of 4.7 *nm/min* and 12 *nm/min*, and various ratios of *In* and *Ga* fluxes.

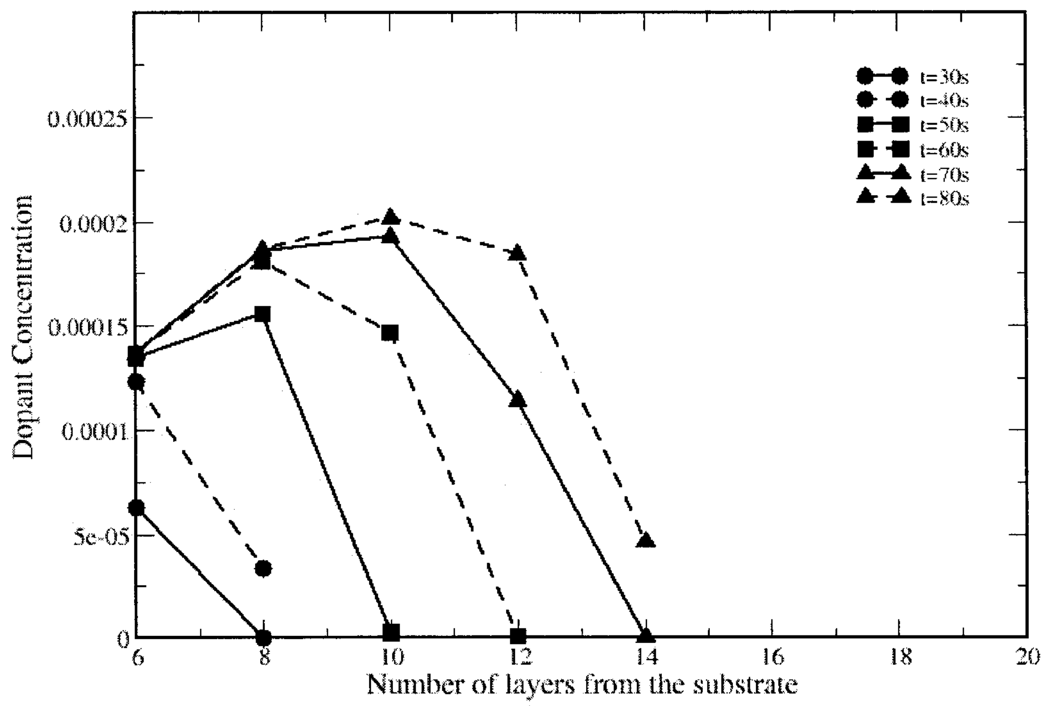

FIGURE 7: Plot of dopant Mg concentration as a function of number of full layers at 600 ^{o}C for various growth times.

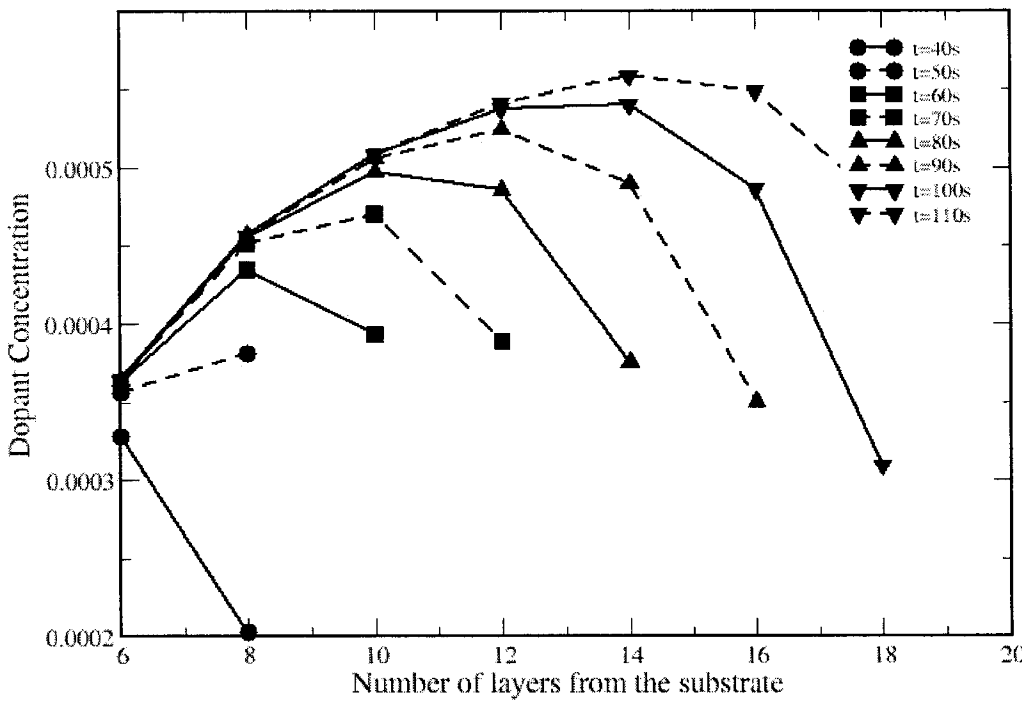

FIGURE 8: Plot of Mg concentration as a function of number of full layers at 680 ^{o}C for various growth times.

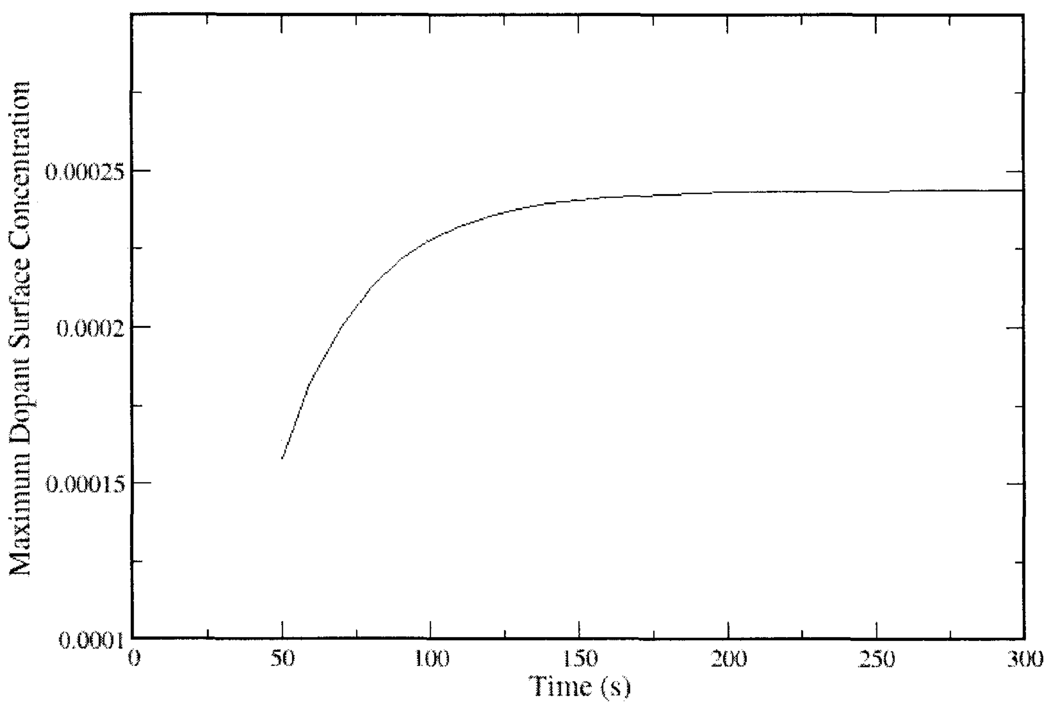

FIGURE 9: The extrapolated data of the *Mg* surface concentration for increased duration of growth

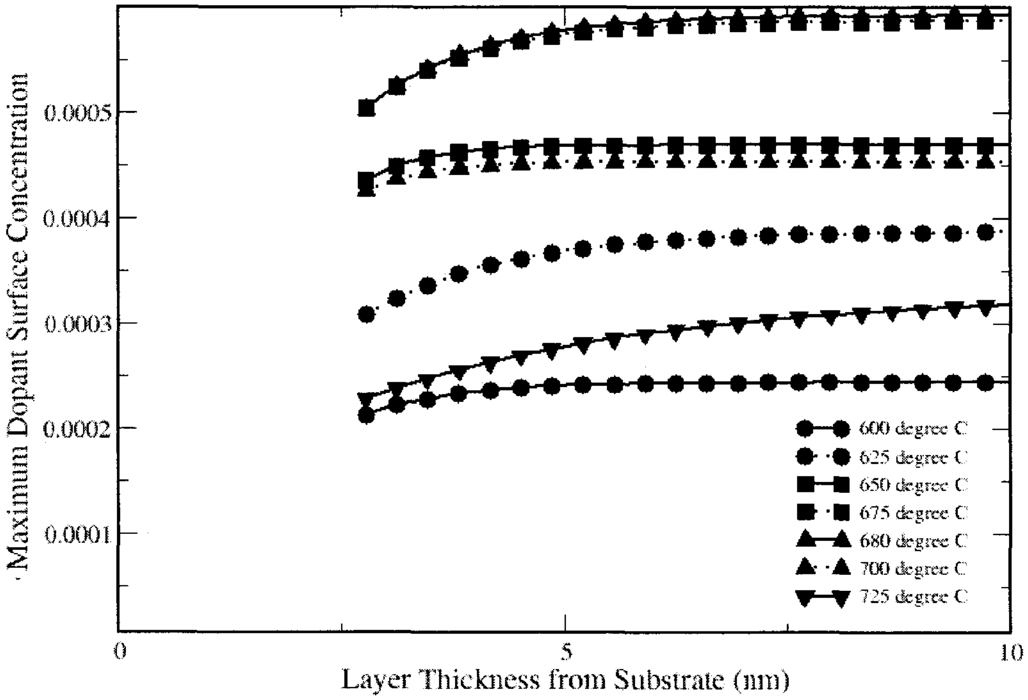

FIGURE 10: The extrapolated data of *Mg* concentration as a function of layer thickness

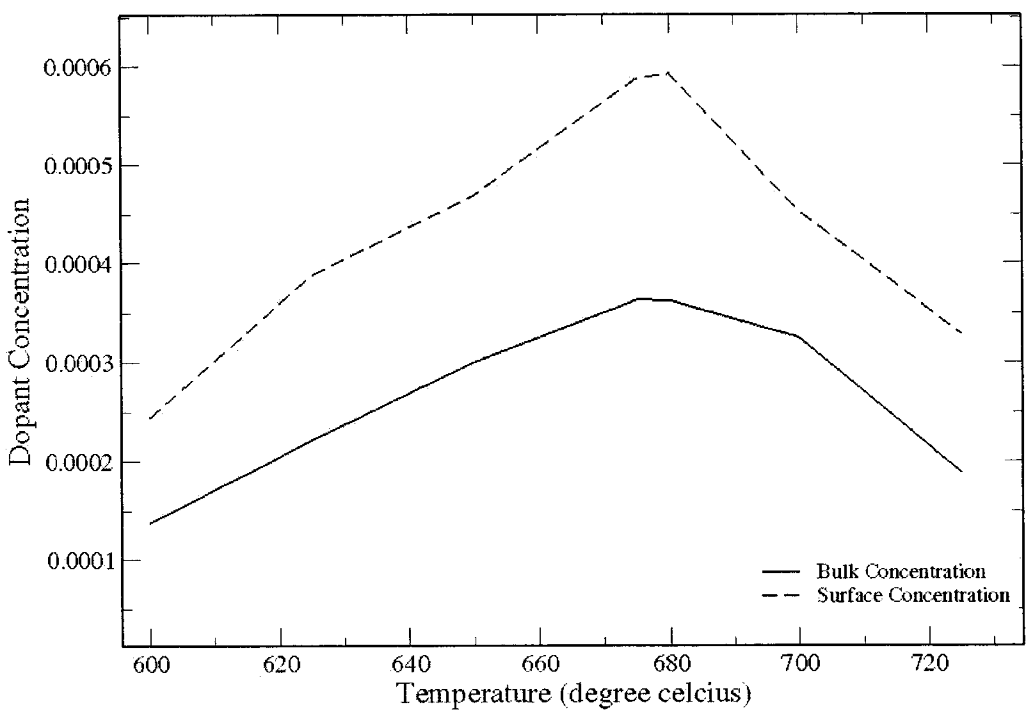

FIGURE 11: Plot of bulk and extrapolated surface concentration of Mg for various growth temperatures

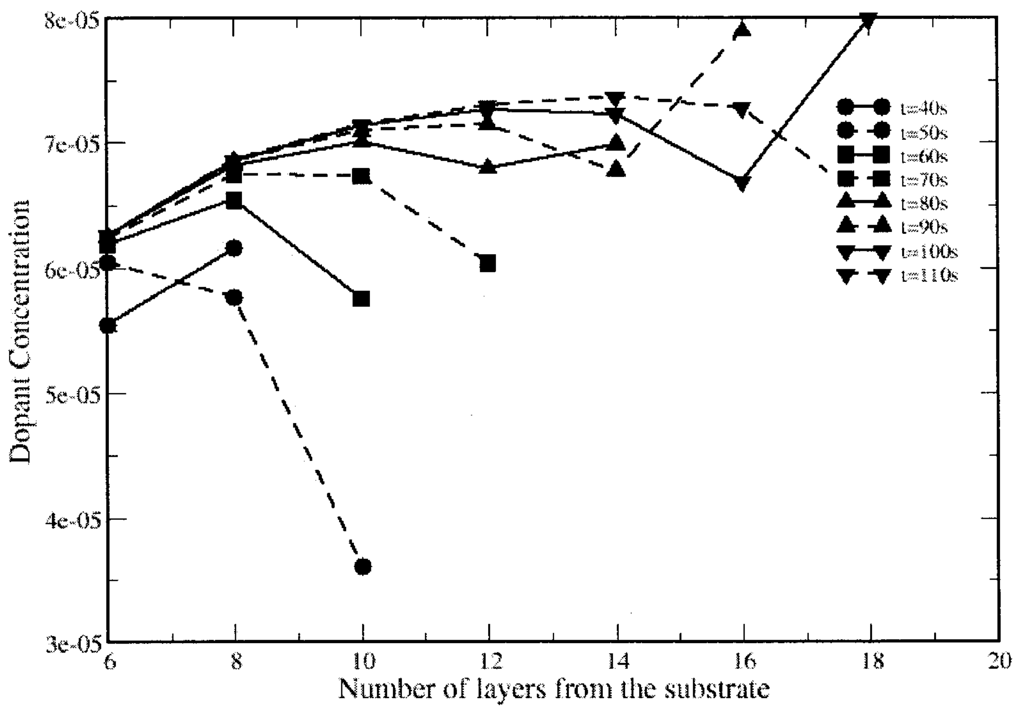

FIGURE 12: *Mg* concentration vs. layer number at 750 ^{o}C. Note the dopant depleted zone for longer growth times.

REFERENCES

[1] M. A. Herman, H. Sitter, "Molecular Beam Epitaxy Fundamentals and Current Status", Springer, Second Edition.

[2] H. Morkoc, "Nitride Semiconductors and Devices", Springer-Verlag, Berlin, (1999).

[3] Dimitris Pavlidis, "III-V Nitride Based Two Terminal Devices For High Power, High Frequency, High Power Applications", Semiconductor Device Research Symposium, 2001 International, 384, (2001).

[4] E. Alekseev, D. Pavlidis, "Microwave potential of *GaN* based Gunn devices", Electronics Letters, 36 (2), 176, (2000).

[5] E. Alekseev, D. Pavlidis, "Large-Signal Microwave Performance of *GaN*-based NDR diode oscillators", Solid-State Electronics, 44 (4), 941, (2000).

[6] T. Paul Chow, Ritu Tyagi, "Wide bandgap compound semiconductors for superior high-voltage unipolar power devices", IEEE Tran. Electron Devices, 41 (8), (1994).

[7] M. A. Khan, M. S. Shur, Q. C. Chen, J. N. Kuznia, "Current/voltage characteristiccollapse in *AlGaN/GaN* heterostructure insulated gate field effect transistors at high drain bias", Electronics Letters IEE, (1994).

[8] G. Fasol, "Room-temperature blue gallium nitride laser diode", Science Magazine, 272 –5269 (21), 1751, (1996).

[9] R. J. Molnar, R. Singh, T. D. Moustakas, "Blue-violet light emitting gallium nitride p-n junctions grown by electron cyclotron resonance assisted molecular assisted epitaxy", Appl. Phys. Lett., 66 (3), 268, (1995).

[10] Shuji Nakamura, "A Bright Future for Blue/Green LEDs: Highly luminous III-V nitride-based devices head for the highway, color displays", IEEE, ISBN 8755-3996, (1995).

[11] Takashi Mukai, Kazunori Takekawa, Shuji Nakamura, "*InGaN* based blue light emitting diodes grown on epitaxially laterally overgrown *GaN* substrates", J. Appl. Phys., 37, L839, (1998).

[12] Takashi Azuhata, Takefumi Homma, Yoshikazu Ishikawa, Shigefusa F. Chichibu, Takayuki Sota, Takashi Mukai, "Current-modulated electroluminescence spectroscopy and its application to *InGaN* single-qunatum well blue and green light emitting diodes", Appl. Phys. Lett., 79 (8), 1100, (2001).

[13] Shuji Nakamura, Takashi Mukai, Masayuki Senoh, "Candela-class high brightness *InGaN/AlGaN* double heterostructure blue light emitting diodes", Appl. Phys. Lett., 64 (13), (1994).

[14] Hiromitsu Sakai, Takashi Koide, Hiroyuki Suzuki, Machiko Yamaguchi, Shiro Yamasaki, Masayoshi Koike, Hiroshi Amano, Isamu Akasaki, "*GaN/GaInN/GaN* double heterostructure leight emitting diodes fabricated using plasma assisted molecular beam epitaxy", Jpn. J. Appl. Phys., 34, L1429, (1995).

[15] Benjamin Damilano, Nicolas Garndjean, Cyril Pernot, Jean Massies, "Monolithic white light emitting diodes based on *InGaN/GaN* multiple quantum wells", Jpn. J. Appl. Phys., 40, L918, (2001).

[16] Nicolas Garndjean, Jean Massies, Mathieu Leroux, Philippe Lorenzini, "Violet *InGaN/GaN* light emitting diodes grown by molecular beam epitaxy using NH_3", Jpn. J. Appl. Phys., 37, L907, (1998).

[17] Daniel L. Barton, Joachim Zeller, B. Scott Phillips, Pei-Chih Chiu, Sabrina Askar, Dong-Seung Lee, Marek Osinski, Kevin J. Malloy, "Degradation of blue *AlGaN/InGaN/GaN* LEDs subjected to high current pulses", IEEE (1995).

[18] S. F. Chichibu, T. Deguchi, T. Sota, K. Wada, S. P.DenBaars, T. Mukai, S. Nakamura, "Properties of quantum well excitons in *GaN/AlGaN* and *InGaN/GaN/AlGaN* UV, blue, green and amber LED structures", Phys. Stat. Sol. (a), 176, 85, (1999).

[19] G. Y. Xu, A. Salvador, W. Kim, Z. Fan, C. Lu, H. Tang, H. Morkoç, G. Smith, M. Estes, B. Goldenberg, W. Yang, S. Krishnankutty, "High speed, low noise ultra violet photodetectors based on *GaN p-i-n* and *AlGaN(p)-GaN(i)-GaN(n)* structures", Appl. Phys. Lett., 71 (15), 2154, (1997).

[20] Shuji Nakamura, Masayuki Senoh, Shin-ichi Nagahama, Naruhito Iwasa, Takao Yamada, Toshio Matsushita, Hiroyuki Kiyoku, Yasunobu Sugimoto, Tokuya Kozaki, Hitoshi Umemoto, Masahiko Sano and Kazuyuki Chocho "*InGaN/GaN/AlGaN* based Laser diodes grown on *GaN* substrates with a fundamental transverse mode", Jpn. J. Appl. Phys., 37, L1020, (1998).

[21] R. Venkatasubramanian, "MBE growth of compound semiconductors: Part I Stochastic Modeling", J. Mater. Res., 7 (5), 1221, (1992).

[22] R. Venkatasubramanian, "MBE growth of compound semiconductors: Part II Applications of Stochastic Model", J. Mater. Res., 7 (5), 1235, (1992).

[23] S. V. Gahisas, A. Madhukar, "Monte-Carlo simulations of MBE growth of III-V semiconductors: The growth kinetics, mechanism, and consequences for the dynamics of RHEED intensity", J. Vac. Sci. Technol. B, 3 (2), 540, (1985).

[24] J. Singh, K. K. Bajaj, "Role of resonant laser enhanced surface kinetics in the low substrate temperature molecular beam epitaxy growth of compound semiconductors: A Mote-Carlo study", Appl. Phys. Lett., 46 (6), 577, (1986).

[25] S. Yu. Karpov, Yu. N. Makarov, M. S. Ramm, "The role of gaseous species in group-III nitride growth", MRS Internet J. Nitride Semicond., 2, 45, (1997).

[26] M. V. Averyanova, S. Yu. Karpov, Yu. N. Markov, I. N. Przhevalskii, M. S. Ramm, R. A. Talalaev, "Theoretical model for analysis and optimization of group III-nitrides growth by molecular beam epitaxy", 1 (31), (1996).

[27] S. Yu. Karpov, R. A. Talalaev, Yu. N. Makarov, N. Grandjean, J. Massies, B. Damilano, "Surface kinetics of *GaN* evaporation and growth by Molecular beam epitaxy", Surface Science, 450, 191, (2000).

[28] R. Held, B. E. Ishaug, A. Parkhomovsky, A. M. Dabiran, P. I. Cohen, "A rate equation model for the growth of *GaN* on *GaN*(000-1) by Molecular beam epitaxy", J. Appl. Phys., 87 (3), 1219, (2000).

[29] Wenning Fu, Rama Venkat, M. Meyyappan, "Theoretical study of *GaN* Molecular beam epitaxy growth using electron cyclotron resonance nitrogen plasma", J. Vac. Sci. Technol. B, 19 (5), 1, (2001).

[30] Nathan Sipe, Rama Venkat, "Modeling *GaN* growth by plasma assisted MBE in the presence of low *Mg* flux", MRS Internet J. Nitride Semicond. Res. 7 (1), (2002).

[31] Huajie Chen, R.M. Feenstra, J. Northrup, Jorg Neugebauer, D. W. Greve, "Indium incorporation and surface segregation during *InGaN* growth by Molecular Beam Epitaxy", MRS Internet J. Nitride Semicond., Res.6, 11 (2001).

[32] R.Averbeck, H. Riechert, "Quantitative model for the MBE growth of ternary nitrides",Phys. Stat. Sol. (a) 176,301 (1999).

[33] S. Guha, N. A. Bojarczuk, F. Cardone, "*Mg* in *GaN*: Incorporation of a volatile species at high temperatures during Molecular Beam Epitaxy", Appl. Phys. Lett., 71 (12), 1685, (1997).

[34] J. M. Myoung, K. Kim, "Effects of growth temperature on *Mg*-doped *GaN* epitaxial films grown by plasma assisted Molecular Beam Epitaxy", J. Vac. Sci. Technol. A, 18 (2), 450, (2000).

[35] T. S. Cheng, C. T. Foxon, N. J. Jeffs, D. J. Dewsnip, L. Flannery, J. W. Orton, S.V. Novikov, B. Ya Ber, Yu A. Kudriavtsev, "Studies of *Mg-GaN* grown by MBE on GaAs(111)B substrates", MRS Internet J. Nitride Semicond., 2 (13), (1997).

[36] T. S. Cheng, S. V. Novikov, C. T. Foxon, J. W. Orton, "Mechanisms of magnesium incorporation into *GaN* layers grown by Molecular Beam Epitaxy", Solid State Communications, 109, 439, (1999).

[37] Wenning Fu, Rama Venkat, "Theoritical Study of *GaN* Molecular Beam Epitaxy growth using ammonia: A rate equation approach", J. Vac. Sci. Technol. B, 18 (3), 1467, (2000).

[38] Shuji Nakamura, Shigefusa F. Chichibu, "Introduction to nitride semiconductor blue lasers and light emitting diodes", Taylor and Francis, (2000).

[39] T. S. Cheng, C. T. Foxon, N. J. Jeffs, O. H. Hughes, B. G. Ren, Y. Xin, P.D. Brown, C. J. Humphreys, A. V. Andranov, D. E. Lacklison, J. W. Orton, M. Halliwell, "Growth of *GaN* films on (001) and (111) *GaAs* surfaces by a modified MBE method", MRS Internet J. Nitride Semicond., 1 (32), (1996).

[40] M. J. Paisley, Z. Sitar, J. B. Posthill, R. F. Davis, "Growth of cubic phase gallium nitride by modified Melecular Beam Epitaxy", J. Vac. Sci. Technol. A, 7 (3), 701, (1989).

[41] T. Lei, M. Fanciulli, R. J. Molnar, T. D. Moustakas, R. J. Graham, J. Scanlon, "Epitaxial growth of zinc blende and wurzitic gallium nitride thin films on (001) Silicon", Appl. Phys. Lett., 59 (8), 944, (1991).

[42] T. Lei, T. D. Moustakas, R. J. Graham, Y. He, S. J. Berkowitz, "Epitaxial growth and characterization of zinc blende gallium nitride on (001) Silicon", J. Appl. Phys., 71 (10), 4933, (1992).

[43] T. D. Moustakas, T. Lei, R. J. Molnar, "Growth of *GaN* by ECR assisted MBE", Physica B, 185, 36, (1993).

[44] R. J. Molnar, T. D. Moustakas, "Growth of gallium nitride electron cyclotron resonance plasma assisted molecular beam epitaxy: The role of charged species", J. Appl. Phys., 76 (8), (1994).

[45] L. T. Romano, B. S. Krusor, R. Singh, T. D. Moustakas, "Structure of *GaN* films grown by molecular beam epitaxy on (0001) sapphire", Journal of Electronic Materials, 26 (3), 285, (1997).

[46] T. D. Moustakas, R. J. Molnar, "Growth and doping of *GaN* films by ECR assisted MBE", Mat. Res. Soc. Symp. Proc., 281, 753, (1993).

[47] Shuichi Kubo, Satoshikurai, Tsunemasa Taguchi, "Homoepitaxial growth of *GaN* thin layer by molecular beam epitaxy with an RF nitrogen plasma", Vacuum, 59, 277, (2000).

[48] M. A. Sanchez-Garcia, E. Calleja, E. Monroy, F. J. Sanchez, F. Calle, E. Munoz, A. Sanz. Hervas, C. Villar, M. Aguilar, "Study of high quality AlN layers grown on Si(111) substrates by plasma assisted molecular beam epitaxy", MRS Internet J. Nitride Semicond., 2 (33), (1997).

[49] E. C. Piquette, P. M. Bridger, Z. Z. Bandic, T. C. McGill, "Growth of III-nitrides by RF assisted molecular beam epitaxy", Mat. Res. Soc. Symp. Proc., 512, 387, (1998).

[50] Z. Yang, L. K. Li, W. I. Wang, "High-quality *GaN* and *AlN* grown by gas-source molecular beam epitaxy using ammonia as the nitrogen source", J. Vac. Sci. Technol. B, 14 (3), 701, (1996).

[51] N. Grandjean, M. Leroux, J. Masries, M. Mesrine, M. Laugt, "Molecular Beam Epitaxy of *GaN* under N-rich conditions using NH_3", Jpn. J. Appl. Phys., 38, 618, (1999).

[52] C. T. Foxon, T. S. Cheng, S. E. Hooper, L. C. Jenkins, J. W. Orton, D. E. Lacklison, S. V. Novikov, T. B. Popova, V. V. Tretyakov, "Molecular beam epitaxy growth kinetics for group III-nitrides", J. Vac. Sci. Technol. B, 14 (3), (1996).

[53] A.N. Alexeev, B. A. Borisov, V. P. Chaly, D. M. Demidov, A. L. Dudin, D. M. Krasovitsky, Yu. V. Pogorelsky, A. P. Shkurko, I. A. Sokolov, M. V. Stepanov, A. L. Ter-Martirosyan, "The growth rate evolution vs. substrate temperature and V/III

ratio during *GaN* MBE using ammonia", MRS Internet J. Nitride Semicond., 4 (6), (1999).

[54] D. E. Crawford, Ruediger Held, A. M. Johnston, A. M. Dabiran, Philip I. Cohen, "Growth rate reduction of *GaN* due to *Ga* surface accumulation", MRS Internet J. Nitride Semicond., 1 (12), (1996).

[55] O. Zsebok, J. V. Thordson, T. G. Andersson, "Surface morphology of MBE- grown *GaN* on *GaAs* (001) as function of the *N/Ga*-ratio", MRS Internet J. Nitride Semicond., 3 (14), (1998).

[56] R. Smith, V. Ramachandran, R. M. Feenstra, D. W. Greeve, A. Ptak, T. Myers, W. Sarney, L. Salamanca-Riba, M. Shin, M. Skowronski, "Surface reconstruction during Molecular beam epitaxy growth of *GaN* (0001)", MRS Internet J. Nitride Semicond., 3 (12), (1998).

[57] Dirk Vogel, Peter Kruger, Johannes Pollman, "Structural and electronic properties of group III-nitrides", Phys. Rev. B, 55 (19), (1997).

[58] C. T. Foxon, T. S. Cheng, S. V. Novikov, D. E. Lacklison, L. C. Jenkins, D. Johnston, J. W. Orton, S. E. Hooper, N. Baba-Ali, T. L. Tansley, V. V. Tretyakov, "Growth and properties of group III-nitrides", J. Cryst. Growth, 150 (1-4), 892, (1995).

[59] K. H. Ploog, O. Brandt, H. Yang, A. Trampert, "MBE growth and characteristics of cubic *GaN*", Thin Solid Films, 306, 231, (1997).

[60] S. Strite, H. Morkoc, "*GaN*, *AlN* and *InN*: A review", J. Vac. Sci. Technol. B, 10 (4), (1992).

[61] Shuji Nakamura, Gerhard Fasol, "The Blue laser Diode-*GaN* based Light Emitters and lasers", Springer –Verlag, Berlin, (1997).

[62] Shuji Nakamura, Takashi Mukai, "High-Quality *InGaN* Films Grown on *GaN* Films", Jpn. J. Appl. Phys., 31, L1457, (1992).

[63] Stephen J. Pearton, "*GaN* and related materials: Optoelectronic properties of semiconductors and superlattices", Gordon and Breach Science Publishers, Volume 2, (1997).

[64] Takashi Mukai, Motokazu Yamada, Shuji Nakamura, "Characteristics of *InGaN*-Based UV/Blue/Green/Amber/Red Light-Emitting Diodes", Jpn. J. Appl. Phys., 38, 3976, (1999).

[65] Huajie Chen, R.M. Freenstra, J. E. Northrup, T. Zywietz, J. Neugebauer, "Spontaneous formation of Indium-rich nano structures on *InGaN* (0001) surfaces", Phys.Rev.Lett.85, 1902-1905 (2000).

[66] J.E Northrup, J. Neugebauer, "Indium-induced changes in *GaN* (0001) surface morphology", Phys. Rev.B, 60, 8473, (1999).

[67] T. Boettcher, S. Einfeldt, V. Kirchner, S. Figge, H. Heinke, D. Hommel, H. Selke, PL. Ryder, "Incorporation of *In* during Molecular beam epitaxy of *InGaN*", Appl. Phys. Lett., 73, 3232, (1998).

[68] Yoshihiro Okamoto, Kazuya Takahashi, Hiromichi Nakamura, Yoshitaka Okada, Mitsuo Kawabe, "Effects of atomic hydrogen on the *In* incorporation in *InGaN* grown by RF Molecular beam epitaxy", Jpn. J. Appl. Phys., 39, L343, (2000).

[69] M. L. O' Steen, F. Fedler, R. J. Haunstein, "A study of the effect of V/III flux ratio and susbstrate temperature on the *In* incorporation efficiency in In_xGa_{1-x}/GaN

heterostructures grown by RF plasma-assisted Molecular beam epitaxy", MRS Internet J. Nitride Semicond. Res. 5S1 (W 3. 27), (2000).

[70] Huajie Chen, R.M. Feenstra, J. Northrup, T. Zywietz, Jorg Neugebauer, D. W. Greve, "Surface structures and growth kinetics of *InGaN* (0001) grown by Molecular beam epitaxy", J. Vac. Sci. Technol. B, 18, 2284, (1992).

[71] Huajie Chen, A. R. Smith, R. M. Feenstra, D. W. Greve, J. E. Northrup, "Scanning tunneling microscopy studies of *InGaN* growth by molecular beam epitaxy", MRS Internet J. Nitride Semicond., Res.S1, G9.5 (1999).

[72] J. Ptak, T. H. Myers, L. T. Romano, C. G. Vandewalle, J. E. Northrup, "Magnesium incorporation in *GaN* grown by RF plasma assisted Molecular beam epitaxy", Appl. Phys. Lett., 78 (3), 285, (2001).

[73] H. Amano, M. Kito, K. Hiramatsu, I. Akasaki, "p-type conduction in *Mg*-doped *GaN* treated with low energy electron beam irradiation (LEEBI)", Jpn. J. Appl. Phys., 28, L2112, (1989).

[74] G. V. Saparin, S. K. Obyden, I. F. Chetverikova, M. V. Chukichev, S. I. Popov, "Anomalous kinetics of cathodoluminescence in *GaN*: *Zn*", Moscow University Physics Bulletin, 38 (3), 56, (1983).

[75] S. Nakamura, N. Iwasa, M. Senoh, T. Mukai, "Hole Compensation Mechanism of *p*-type *GaN* Films", Jpn. J. Appl. Phys., 31, 1258, (1992).

[76] T. H. Myers, A. J. Ptak, Lijun Wang, N. C. Giles, "Magnesium and beryllium doping during RF plasma MBE growth of *GaN*", Inst. of pure and Appl. Phys. Conference series, 1, 451, (2000).

[77] C. T. Foxon, T. S. Cheng, N. J. Jeffs, J. Dewsnip, L. Flannery, J. W. Orton, I. Harrison, S. V. Novikov, B. Ya. Ber, Yu. A. Kudriavtsev, "Studies of *p-GaN* grown by MBE on GaAs (111) B", J. Cryst. Growth, 189/190, 516, (1998).

[78] B. Ya. Ber, Yu. A. Kudriavtsev, A. V. Merkulov, S. V. Novikov, D. E. Lacklison, J. W. Orton, T. S. Cheng, C. T. Foxon, "Secondary ion mass spectroscopy investigations of magnesium and carbon doped gallium nitride films grown by molecular beam epitaxy", Semicond. Sci. Technol., 13 (1), 71, (1998).

[79] D. J. Dewsnip, J. W. Orton, D. E. Lacklison, L. Flannery, A. V. Andrianov, I. Harrison, S. E. Hooper, T. S. Cheng, C. T. Foxon, S. V. Novikov, B. Y. Ber, Y. A. Kudriavtsev, "p and n-type doping of MBE grown cubic *GaN/GaAs* epilayers", Semicond. Sci. Technol., 13, 927, (1998).

[80] S. Guha, N. A. Bojarczuk, F. Cardone, "*Mg* in *GaN*: Incorporation of a volatile species at high temperatures during molecular beam epitaxy", Appl. Phys. Lett., 71, 1685, (1997).

[81] M. S. Brandt, N.M. Johnson, R. J. Molnar, R. Singh, T. D. Moustakas, "Hydrogenation of p-type gallium nitride", Appl. Phys. Lett., 64, 2264, (19994).

[82] J. M. Myoung, K. H. Shim, O. Gluschenkov, C. Kim, K. Kim, S. Kim, S. G. Bishop, "Effect of growth temperature on the properties of *p*-type *GaN* grown by plasma-assisted Molecular beam epitaxy", J. Cryst. Growth, 182, 241, (1997).

[83] Guido Mula, Bruno Daudin, Christoph Adelmann, Philippe Peyla, "MBE growth of *GaN* films of *GaN* films in presence of surfactants: The effects of *Mg* and *Si*", MRS Internet J. Nitride Semicond. Res. 5S1 (W 3. 35), (2000).

[84] Bruno Daudin, Guido Mula, Philippe Peyla, "*Mg*-modified surface kinetics of the *GaN* growth by Molecular beam epitaxy", Phys. Rev. B, 61 (15), (2000).

[85] Z. Liliental-Weber, M. Benamara, W. Swider, J. Washburn, I. Grzegory, S. Porowski, R. D. Dupuis, C. J. Eiting, "*Mg* segregation, difficulties of p-doping in *GaN*", MRS Internet J. Nitride Semicond., Res.5S1, W9.7 (2000).

[86] H. M. Ng, D. Doppalapudi, D. Korakakis, R. Singh, T. D. Moustakas, "MBE growth and doping of III-V nitrides", J. Cryst. Growth, 189/190, 349, (1998).

[87] D. J. As, K. Lischka, "Heteroepitaxy of doped and undoped cubic group III nitrides", Phys. Stat. Sol (a), 176, 475, (1999).

VITA

Graduate College
University of Nevada, Las Vegas

Irena Vidhya Mabel Stanley

Local Address:
4248 Chatham Circle
Las Vegas, NV 89119

Degree:
Bachelor of Science
Electronics and Communication Engineering, 2001
University of Madras, India

Thesis Title:
Theoretical Study of Segregation Kinetics of *In* in *InGaN* and *Mg* in *Mg-GaN* Grown by Molecular Beam Epitaxy

Publication:
Irena Stanley *et. al.*, Theoretical Study of *In* Desorption and Segregation Kinetics in MBE Growth of *InGaAs* and *InGaN* , Journal Of Crystal Growth, Volume 251/1-4.

Thesis Examination Committee:
Chairperson, Dr. Rama Venkat, Ph. D.
Committee Member, Dr. Shahram Latifi, Ph. D., P. E.
Committee Member, Dr. Sahjendra Singh, Ph. D.
Graduate faculty Representative, Dr. Ajoy K. Datta, Ph. D.